Control of pili synthesis and putrescine homeostasis in *Escherichia coli*

Running title: *E. coli* surface motility and putrescine homeostasis

Iti Mehta[1#], Jacob Hogins[1#], Sydney Hall[1], Gabrielle Vragel[1], Sankalya Ambagaspitiye[1], Philippe Zimmern[2], Larry Reitzer[1]*

[1] Department of Biological Sciences, UT Dallas, Richardson, Texas

[2] Department of Urology, the University of Texas Southwestern, Dallas, Texas, USA

*Author for correspondence: Tel: 972-883-2502; Fax: 972-883-2409; reitzer@utdallas.edu

# Authors contributed equally and should be considered co-first authors

Keywords: polyamines, putrescine, surface motility, pili, *Escherichia coli*, putrescine homeostasis

Summary

Polyamines are biologically ubiquitous cations that bind to nucleic acids, ribosomes, and phospholipids and, thereby, modulate numerous processes, including surface motility in *Escherichia coli*. We characterized the metabolic and transcription factors that contribute to polyamine-dependent control of surface motility. Genetic analysis showed that surface motility required type 1 pili and the simultaneous presence of two independent putrescine anabolic pathways and that putrescine transport and catabolism modulated surface motility. The results of an immunological assay for FimA—the major pili subunit, reverse transcription quantitative PCR of *fimA*, and transmission electron microscopy confirmed that pili synthesis required putrescine. RNAseq analysis of a parental and putrescine-deficient mutant and a follow-up genetic analysis suggested that H-NS was the putrescine-responsive regulator of pili synthesis and surface motility. The RNAseq results also showed that low putrescine increased transcripts for genes of arginine synthesis and transport systems for magnesium and phosphate, and decreased transcripts of genes for oxidative energy metabolism and iron transport. We conclude that (a) putrescine controls pili synthesis and surface motility possibly via the transcriptional regulator H-NS, and (b) a complex homeostatic network, which can rewire metabolism, controls putrescine concentrations. During a urinary tract infection, the polyamine putrescine is present in urine and pili are required for the binding of bacteria to the bladder epithelium. Because of its control of pili synthesis and energy metabolism, putrescine is likely to contribute to the establishment and maintenance of urinary tract infections associated with uropathogenic *Escherichia coli*.

36 ## Introduction

37 Polyamines are flexible aliphatic cations that are found in virtually all organisms. *E. coli*
38 contains putrescine (1,4-diaminobutane) and lesser amounts of spermidine (N-(3-aminopropyl)-
39 1,4-diaminobutane), and cadaverine (1,5-diaminopentane) (1, 2). Both the pathways and enzymes
40 of polyamine synthesis are redundant (Fig. 1). Strains that lack eight of these genes do not contain
41 detectable polyamines, grow slowly aerobically, and do not grow anaerobically (3). Polyamines
42 interact with nucleic acids and phospholipids, can affect chromosome and ribosome structure,
43 ribosome-mRNA interactions, and protein and nucleic acid elongation rates (4). Polyamines
44 modulate, but are not required for, protein synthesis (5) and expression of hundreds of genes (6).
45 A major mechanism of polyamine-dependent regulation is translational control of genes for 18
46 major transcription regulators: four of the seven σ factors – σ^{18} (FecI), σ^{24} (RpoE), σ^{38} (RpoS), and
47 σ^{54} (RpoN); three histone-like DNA-binding proteins (Fis, H-NS, and StpA); and CpxR, Cya, Cra,
48 and UvrY (5, 6).

49 Polyamines control flagella-dependent surface motility of *Proteus mirabilis* and pili-
50 dependent surface motility (PDSM) of *E. coli*: the latter has been reported to require the polyamine
51 spermidine (7, 8). While reconstructing putrescine-deficient strains to characterize the basis for
52 the anaerobic growth defect, we noticed that a mutant unable to synthesize spermidine moved
53 normally, while mutants lacking enzymes of putrescine synthesis moved poorly. We characterized
54 the role of polyamines on *E. coli* surface motility and pili synthesis by genetic analysis, ELISA
55 assays, RT-qPCR, electron microscopy, and RNAseq. We showed that PDSM and pili synthesis
56 required two independent pathways of putrescine synthesis, but did not require spermidine, and
57 was modulated by putrescine transport and catabolism. In addition to confirming that putrescine
58 controlled pili synthesis, results from an RNAseq analysis identified regulators that mediated

putrescine-dependent control, and, unexpectedly, suggested a putrescine homeostatic network that rewires metabolism to maintain intracellular putrescine.

Results

Pili-dependent surface motility (PDSM) of W3110.

While characterizing mutants lacking putrescine synthetic enzymes, we found that some strains were defective in surface motility. Because any single laboratory strain may have properties that result from unintended laboratory evolution, we assessed nine strains for their surface motility pattern. Five strains covered a plate in 12-18 hours, while four did not traverse a plate in 36 hours. The slow-moving strains generated genetically stable fast-moving variants which suggests that the former were ancestral. Our lab strain of W3110 moved slowly, and among the slow movers showed the least variability in spreading diameter and generated fewer fast-moving variants. Its outward movement formed concentric rings, with alternating phases of movement and consolidation/growth (Fig 2A). Deletion of *fimA*, which codes for the major type 1 pili subunit, abolished the oscillatory pattern and reduced, but did not eliminate, surface motility, but deletion of *fliC* which encodes the major flagellum subunit did not affect surface motility (Fig. 2A). Electron microscopy confirmed that W3110-LR isolated from surface motility plates possessed pili (Fig. 2B). None of >500 cells expressed flagella. A mixed population of elongated (3-4 μm) and non-elongated (<2 μm) cells were visible, and pili were mostly associated with elongated cells. Furthermore, W3110 surface motility requires glucose (9) which should prevent flagella synthesis via inhibition of cyclic AMP synthesis (10). We confirmed that glucose controlled flagella synthesis in W3110 by its suppression of swimming motility (Fig 2C). A W3110-LR derivative with deletions of both *fliC* and *fimA* still exhibited outward movement on a surface motility plate

82 (Fig 2A), but electron microscopy showed the absence of appendages (Fig. 2C). In summary,
83 genetics, electron microscopy, and a glucose requirement show that W3110 surface motility
84 requires pili.
85
86 **PDSM required two independent putrescine synthesis pathways.**
87 We examined PDSM requirements for polyamine anabolic pathways. A major putrescine
88 biosynthetic pathway is ornithine decarboxylation either by the constitutive SpeC or the low-pH
89 inducible SpeF. The Δ*speC* and Δ*speF* mutants moved as well as the parental strain, but a Δ*speC*
90 Δ*speF* double mutant moved less well (Figure 3). SpeA (arginine decarboxylase) and SpeB
91 (agmatinase) catalyze an alternate two-step putrescine synthetic pathway (Fig 1) (11): deletion of
92 either gene reduced surface motility (Figure 3). The Δ*speA*, Δ*speB*, and Δ*speC* Δ*speF* strains grew
93 as well as the parental strain (Supplemental Figure 1A) and had normal swimming motility
94 (Supplemental Figure 1B). A Δ*speE* mutant, which lacks the enzyme for spermidine synthesis,
95 moved on a surface as well as the parental strain (Fig 3).
96 Supplemental putrescine at 1 mM restored surface motility of a *speB* mutant (Figure 4A)
97 and a *speA* mutant (not shown). Spermidine did not restore wild type movement and, also, caused
98 an unusual pattern of movement in the parental strain (Figure 4B). These exogenous concentrations
99 of putrescine and spermidine had no effect on growth rates in liquid motility medium (not shown).
100 In summary, PDSM required the simultaneous presence of two independent pathways of putrescine
101 synthesis but did not require spermidine.
102
103 **Loss of putrescine transport systems affected surface motility.**

104 Putrescine transport may maintain an appropriate intracellular putrescine concentration,
105 because *E. coli* secretes putrescine (12). *E. coli* has several putrescine transport systems (13, 14).
106 Mutants lacking the PlaP and PotF putrescine transporters had 50% and 40% reduced surface
107 motility, respectively, and lost the concentric ring pattern (Figure 5A). Loss of the PotE and PuuP
108 transporters affected neither the movement diameter (Figure 5B) nor concentric ring formation
109 (Figure 5A). We note that *potE* and *plaP* are more highly expressed than *potE* and *puuP* (85, 64,
110 17, and 6 counts per million transcripts, respectively) for W3110 grown in liquid motility medium
111 (15). We conclude that extracellular putrescine and its transport contribute to PDSM.
112
113 **Putrescine catabolism affected surface motility.**
114 Because putrescine catabolism modulates intracellular putrescine concentrations (16, 17),
115 we examined PDSM in putrescine catabolic mutants. The major putrescine catabolic pathway is
116 initiated with putrescine glutamylation (reactions 6-9, and 4-5, Fig 6A), and a second pathway
117 initiates with putrescine deamination (reactions 1-5, Fig 6A) (17). Deletion of either *puuA* or *patA*
118 which code for the first enzymes of their respective pathways did not affect surface motility (Fig
119 6B). A double mutant moved less well which was unexpected because the proposed higher
120 intracellular putrescine should have stimulated PDSM. Consistent with the stimulatory effect of
121 putrescine, loss of *puuR* which codes for the repressor of PuuA-initiated pathway genes (17),
122 impaired PDSM (Fig 6B). One possible explanation to reconcile these seemingly contradictory
123 results is that an optimal polyamine concentration stimulates PDSM, and a high concentration is
124 inhibitory. Experiments that are described in the next section test this possibility.
125
126 **High putrescine reduced expression of pili genes.**

127 High putrescine inhibits translation of some mRNAs, and high spermidine, a product of
128 putrescine metabolism, inhibits growth (18, 19). If the phenotype of the Δ*patA* Δ*puuA* double
129 mutant results from spermidine toxicity, then loss of spermidine synthase (SpeE) should reverse
130 the phenotype. This prediction was not met which argues against spermidine toxicity (Fig 6C).
131 For the *speB* mutant, 1 mM putrescine stimulated PDSM, and 4 mM putrescine was slightly
132 inhibitory but eliminated the ring pattern (Fig 7AB). The concentric ring pattern was observed
133 with 1 mM, but not 4 mM putrescine. Indirect enzyme linked immunosorbent assays (ELISAs)
134 against FimA showed that the level of FimA in the *speB* mutant at 1 mM putrescine was higher
135 than with 4 mM putrescine (Fig. 7C). Variation of supplemental putrescine did not affect FimA in
136 the parental strain (Fig. 7C).
137 To test transcriptional regulation of pili expression by putrescine, we examined transcript
138 levels by RT-qPCR. Optimal *fimA* transcription occurred at 1 mM putrescine in the *speB* mutant
139 (Fig 7D). Transmission electron microscopy (TEM) showed that pili expression was highest for
140 the *speB* mutant at 1 mM putrescine (Fig. 8), moderate at 0.1- and 4-mM putrescine, and
141 undetectable without putrescine. The cells grown with 4 mM putrescine were shorter and thinner,
142 which suggests a stress, possibly mimicking osmotic stress. From these results and those in the
143 previous section, we conclude that pili expression required an optimal putrescine concentration.
144

145 **RNAseq analysis identified H-NS as a possible mediator of putrescine-dependent control.**

146 To determine whether putrescine affects transcription of genes whose products control
147 *fim* operon expression (20), we performed RNAseq analysis of the parental and *speB* strains
148 grown with and without 1 mM putrescine. The transcriptomes of the parental strain both with
149 and without putrescine and the *speB* mutant with 1 mM putrescine were highly similar with R^2

150 values of 0.950 and 0.954, respectively, based on expression graphs comparing the
151 transcriptomes of the parental strain in both conditions to the *speB* mutant strain (Supplemental
152 Figure 2). Compared to the transcriptome of the *speB* mutant grown without putrescine, the
153 transcriptomes of the parental strain without putrescine (R^2 = 0.796), the parental with 1 mM
154 putrescine (R^2 = 0.786), and the *speB* mutant with 1 mM putrescine (R^2 = 0.820) differed
155 substantially. A multidimensional scaling plot and a plot of the 100 most variable genes further
156 visualize these interactions (Fig 9A and 9B).
157 When compared to the parental strain, the *speB* mutant grown without putrescine had 310
158 downregulated genes and 159 upregulated genes with at least four-fold differential expression
159 and FDR < 0.05. Transcripts for the putrescine-responsive *puuAP* and *puuDRCBE* operons,
160 which specify genes of the major putrescine catabolic pathway, were reduced from 1.6- to 14-
161 fold (FDR ≤ 0.02) in the *speB* mutant (Supplemental Table 1), which implies lower intracellular
162 putrescine. Deletion of *speB* reduced transcripts for genes of the *fimA* operon and *fimE*, but not
163 of *fimB* (Fig 10A). Furthermore, loss of *speB* affected some of the known positive effectors that
164 control *fim* operon expression which include Fis, H-NS, IHF, Lrp, and QseB (21). Transcripts
165 from *hns* were reduced, transcripts from *ihfA* and *ihfB* were not affected, and transcripts from *fis*,
166 *lrp*, and *qseB* were increased when *speB* was deleted (Fig 10B). Loss of *speB* also increased
167 transcripts from *lrhA* which codes for a positive effector of *fimE*. Loss of several of these
168 regulators eliminated PDSM which was expected (Fig 10C). H-NS may mediate putrescine-
169 dependent control of pili synthesis. However, given the numerous effects of loss of *speB*, a
170 generalized dysregulation of several major transcription factors may also produce a less-than-
171 optimal constellation of regulators.
172

173 **Evidence for a homeostatic network that maintains intracellular putrescine.**

174 The gene expression changes resulting from loss of *speB* unexpectedly suggested
175 compensatory mechanisms for low putrescine. The transcript differences for all genes are
176 provided in Supplemental Table 1, and for selected genes in Table 1. A gene expression pattern is
177 summarized in Fig 11. The *speB* mutant had more transcripts from (a) genes of arginine and
178 ornithine carboxylase, (b) all genes of ornithine and arginine synthesis from glutamate, and (c)
179 genes for three separate putrescine transport systems. The *speB* mutant also had fewer transcripts
180 from the *sap* operon which codes for a putrescine exporter (12), and from *rpmH* and *rpsT*, whose
181 products inhibit ornithine and arginine decarboxylase (22). The net effect of these changes
182 should be to increase intracellular putrescine: follow the solid arrows in the left half of Fig. 11.

183 Loss of *speB* also affected pathways of energy metabolism. For instance, glutamate and
184 α-ketoglutarate are at a branch point in metabolism which can either provide putrescine
185 precursors or generate energy. The *speB* mutant had fewer transcripts for metabolic genes coding
186 for all citric acid cycle enzymes, NADH dehydrogenase I (the entire *nuo* operon), cytochrome
187 oxidase (the *cyo* operon), and several genes of menaquinone (the *menFDHBCE* operon),
188 ubiquinone, and heme synthesis. In addition to these differences, the *speB* mutant also had fewer
189 transcripts for all genes of iron acquisition, which is consistent with diminished energy
190 generation. In sum, this pattern suggests that low putrescine diverts metabolic flux from energy-
191 generating pathways to putrescine synthesis.

192 One of the most differentially expressed gene between the parental and *speB* mutant
193 strains was *mgtA* which had 60-fold more transcripts in the *speB* mutant and codes for the major
194 magnesium transporter. The *speB* mutant also had more transcripts for several phosphate

195 assimilation genes, including *phoB* which codes for the response regulator of phosphate
196 limitation.
197

198 ## Discussion

199 PDSM and pili synthesis required putrescine synthesis and were affected by putrescine
200 degradation and transport, as well as several transcription factors, which implies that numerous
201 factors control intracellular putrescine concentrations. The effect of loss of putrescine transport
202 systems on PDSM implicates extracellular putrescine on putrescine homeostasis. A requirement
203 for the SpeA-SpeB pathway implicates extracellular arginine since SpeA is mostly periplasmic
204 (23). The role of both putrescine synthesis and degradation suggests rapid adjustments to
205 fluctuating putrescine concentrations. Numerous transcription factors control pili synthesis. Of
206 these, only the gene for H-NS had fewer transcripts in the *speB* mutant, which is consistent with
207 H-NS mediating putrescine-dependent control. This conclusion is not considered strong because
208 of the only two-fold transcript reduction, and because of numerous changes in transcripts for other
209 potential pili regulations in the *speB* mutant, albeit in the wrong direction. Therefore, we cannot
210 exclude a general regulatory dysfunction mediated by depleted levels of putrescine as the basis for
211 loss of pili synthesis.

212 An unexpected observation was that the *speB* mutant had more transcripts for genes whose
213 products will maintain intracellular putrescine, i.e., compensatory mechanisms for low
214 intracellular putrescine (Figure 11). Conversely, loss of *speB* lowered transcripts for many genes
215 of energy metabolism and all genes of iron acquisition. This gene expression pattern suggests a
216 diversion of metabolism away from energy generation and toward putrescine synthesis, i.e., a
217 prioritization of putrescine synthesis over aerobic energy metabolism.

218 We also propose that other changes are also compensatory mechanisms for low intracellular
219 putrescine, specifically, more transcripts for genes coding for magnesium and phosphate transport
220 systems in the *speB* mutant. To the extent that magnesium can directly replace putrescine, e.g.,
221 binding to nucleotides and RNA (24), magnesium could compensate for low putrescine. Our
222 observations confirm those of J. Slauch and colleagues on an inverse correlation between
223 intracellular magnesium and polyamines in *Salmonella* (25). They proposed an overall divalent
224 cation homeostasis maintained by either magnesium or the polyamines (25). A rationale for the
225 effect on phosphate metabolism is not obvious but considering the effects of low putrescine on
226 energy metabolism, increased phosphate transport may be an adjustment to changes in energy
227 metabolism. In any case, the substantial changes in gene expression due to low putrescine suggest
228 multiple compensatory mechanisms, and a homeostatic gene network which because of effects on
229 metabolic genes can rewire metabolism.

230 In contrast to our results, a thorough and well-designed study showed that *E. coli* PDSM
231 requires spermidine instead of putrescine (8). The differences between the studies were strain
232 backgrounds, media (glucose-LB vs glucose-tryptone), and incubation temperature (33º vs 37º).
233 We found PDSM results for 37º incubations were highly variable and resulted in numerous fast-
234 moving variants. Since growth at the higher temperature is faster, and faster growth is associated
235 with higher putrescine, we propose that growth at 37º results in an inhibitory putrescine
236 concentration. In this case, spermidine would be stimulatory because of its known inhibition of the
237 putrescine biosynthetic enzymes SpeA and SpeC (26, 27) and subsequent reduction of intracellular
238 putrescine to an optimal concentration.

239 The transcript changes observed in our study were different from those in the only other
240 systematic study of putrescine's effect on *E. coli* gene expression (6). Both studies had almost

241 identical experimental design: 1.0- or 1.14-mM putrescine was added to either a *speB* or *speB speC*
242 mutant, respectively. Differences in strains, growth media (minimal media vs tryptone-containing
243 media), and growth temperature (33º vs 37º) could account for the discrepancy in results. The most
244 crucial difference could be the growth media: Igarashi and colleagues grew bacteria in a minimal
245 medium, while we grew bacteria in an amino acid-containing medium that was required for surface
246 motility. We propose that the slower growth in minimal medium correlates with higher guanosine
247 tetraphosphate and in turn counters and obscures many growth-stimulatory putrescine effects.
248 In contrast, the growth stimulation from the amino acids in our medium would not counter
249 putrescine effects and would essentially allow detection of effects caused solely by changes in
250 putrescine concentrations. Regardless of the explanation, common results can be interpreted as
251 core responses to putrescine limitation. Both studies observed that low putrescine increased
252 transcripts for genes of arginine synthesis and magnesium transport, and reduced transcripts for
253 the *sdhCDAB-sucABCD* operon which codes for TCA cycle enzymes. The link between putrescine
254 and arginine synthesis is probably mediated by the ArgR repressor because *argR* transcripts are
255 2.5-fold lower (FDR = 0.0004) in the *speB* mutant (Supplemental Table 1). Cyclic AMP may
256 mediate putrescine-dependent control of the *sdh-suc* operon because putrescine controls
257 translation of *cya* mRNA, which codes for adenylate cyclase, and cyclic-AMP controls the
258 *sdhCDAB-sucABCD* operon. As noted above, the link between putrescine and magnesium
259 transport is a recent observation (25).
260 Several results implicate putrescine in *E. coli* virulence during urinary tract infections.
261 First, pili-dependent binding to the urothelium is an essential step for uropathogenic *E. coli* (28).
262 Second, putrescine is present in urine from infected, but not healthy individuals (29, 30). Third,
263 urinary putrescine can result from UPEC growth in urine (30) and urothelial pathophysiology (31).

264 Putrescine's possible role in virulence is seemingly contradicted by the observation that a *speB*
265 mutant outcompetes the parental CFT073 in the bladder of mice, i.e., less putrescine synthesis
266 enhanced virulence (32). A majority of uropathogenic *E. coli* are associated with phylogenetic
267 group B2—including CFT073, whereas most *E. coli* lab strains, such as W3110, are group A.
268 Group B2 strains lack genes for the major putrescine catabolic pathway and have significantly
269 higher transcripts for genes coding for SpeA and SpeB (15). Both observations suggest that the
270 cytoplasmic putrescine concentration is higher in group B2 strains. We propose that the putrescine
271 concentration in group B2 strains is normally in the inhibitory range for pili synthesis, and that
272 loss of SpeB reduces putrescine to a level that stimulates pili synthesis. Regardless of the
273 explanation, putrescine is likely to be important during urinary tract infections, but aspects of
274 putrescine control of pili synthesis and other processes could be different in uropathogenic *E. coli*
275 and is worth further examination.
276

277 ## Experimental Procedures

278 **Strains.** All strains used for growth rate determinations and motility assays were derivatives of *E.*
279 *coli* K-12 strain W3110 and are listed in Table 2. Great variations exist in standard lab strains,
280 including W3110, from different labs. We tested nine strains, most from the Coli Genetic Stock
281 Center, and chose our lab strain because of relative genetic stability and more quantitatively
282 reproducible results. Our strain originated from the lab of Jon Beckwith in the 1960s via the lab of
283 Boris Magasanik where it had been stored in a room temperature stab until the mid-1980s, at which
284 time it was revived and frozen at -80° C. Although mutations may have accumulated during
285 storage, its transcriptome is similar to that of other strains of the same phylogenetic group when
286 grown in motility medium (15). To construct the mutant strains, the altered allele was obtained

287 from the Keio collection in which the gene of interest had been deleted and replaced with an
288 antibiotic resistance gene (33). The marked deletion allele was transferred into W3110 by P1
289 transduction (34). The antibiotic gene was removed as described which generated an in-frame
290 deletion (35).
291
292 **Media and Growth Conditions.** For P1 transductions and plasmid transformation experiments,
293 cells were grown in standard LB liquid medium (1% tryptone, 1% NaCl and 0.5% yeast extract,
294 pH 7.0) at 37°C. Antibiotics were used for selection at concentrations of 25 μg/mL (both
295 chloramphenicol and kanamycin). For growth analysis, bacteria were grown in liquid motility
296 medium (0.5% glucose, 1% tryptone, and 0.25% NaCl) which we refer to as GT medium. Starter
297 cultures (typically 6–12 h incubation) were grown in GT medium, harvested by centrifugation,
298 washed twice with phosphate buffered saline and re-suspended in GT medium before inoculation.
299 The cells were then grown at 37° C in aerobic conditions (shaking at 240 rpm) and the turbidity
300 was measured every thirty minutes. Cell growth was measured in Klett units using a Scienceware
301 Klett colorimeter with a KS-54 filter. 100 Klett units represent an OD_{600} value of about 0.7.
302
303 **Surface motility assay.** For a standard surface motility assay, single colonies from fresh plates
304 (streaked out from frozen stocks a day before) were inoculated in GT medium for six hours at
305 37° C in aerobic conditions (shaking at 240 rpm). 30 ml of autoclaved GT medium with 0.45%
306 agar (Eiken, Tokyo, Japan) was poured into sterile polystyrene petri-dish (100 mm X 15 mm)
307 and allowed to solidify at room temperature for approximately six hours. Then, 1 μL of the pre-
308 motility growth medium was inoculated at the center of the agar plate and incubated at 33° C for
309 36 hrs. Each experiment was performed in triplicate and pictures were taken after 36 hours.

310 Surface motility was extremely sensitive to humidity. Opening the incubator before 36 hours
311 resulted in movement cessation. The surface motility assay was performed at 33º C because
312 results from incubations at 37º C were highly variable and the cultures more frequently generated
313 genetically stable fast-moving variants.
314
315 **Swim assay.** The media and culturing for swimming motility is identical to that for surface
316 motility, except that the plates contained 0.25% agar and were solidified at room temperature for
317 about one hour before inoculation. Then, 1 μL of the culture was stabbed in the center of this
318 swim agar plate and incubated at 33° C for 20 hours. Each experiment was performed in
319 triplicate.
320
321 **Transmission electron microscopy.** Cells from surface motility plates were collected and fixed
322 with 2.5% glutaraldehyde. Bacteria were absorbed onto Foamvar carbon-coated copper grids for
323 1 min. Grids were washed with distilled water and stained with 1% phosphotungstic acid for 30
324 s. Washed and stained grids were dried at 37ºC for 10 minutes. Samples were viewed on a JEOL
325 1200 EX transmission electron microscope at the University of Texas Southwestern (Figure 2)
326 and the University of Texas at Dallas (Figure 8).
327
328 **ELISA analysis.** Cells were grown overnight in 5 mL GT media followed by a 2-hour growth in
329 GT media with 0.0, 0.1, 1.0, or 4.0 mM putrescine. Cells were then lysed using a 24-gauge
330 needle. The cell lysate was diluted to a concentration of 1 mg/mL protein (based on A280) in pH
331 9.6 coating buffer (3 g Na_2CO_3, 6 g $NaHCO_3$, 1000 mL distilled water) and then coated onto the
332 walls of a 96-well plate by incubating overnight at 4°C. The wells were rinsed 3 times with PBS

333 and further blocked using coating buffer with 1% bovine albumin overnight at 4°C. The
334 following day, wells were rinsed 3 times with PBS, and primary antibodies to FimA or RpoD
335 were added following supplier directions. After a 2-hour room temperature incubation, secondary
336 antibodies conjugated to HRP were added and incubated for a further two hours. HRP was
337 activated using the TMB substrate kit (Thermo-34021) following the provided protocol.
338 Expression was read on a BioTek plate reader based on the provided kit protocol. Data was
339 blanked to wells only treated with bovine albumin then normalized to RpoD. Data was generated
340 from technical and biological triplicates.
341
342 **DNA isolation and genome assembly and annotation for W3110.** DNA was isolated based on
343 previous established protocols (36). Short reads were sequenced at the SeqCenter (Pittsburgh,
344 Pennsylvania) using Illumina tagmentation-based and PCR-based DNA prep and custom IDT
345 indices targeting inserts of 280 bp without further fragmentation or size selection steps. The
346 Illumina NovaSeq X Plus sequencer was ran producing 2X151 paired-end reads.
347 Demultiplexing, quality control, and adapter trimmer was performed with bcl-convert (v4.2.4).
348 Total Illumina Reads (R1+R2): 4059078 with 553087045 bps >Q30.
349 Long reads were prepared using the PCR-free Oxford Nanopore Technologies ligation
350 sequencing kit with the NEBNext companion module. No fragmentation or size selection was
351 performed. Long read libraries were performed using R10.4.1 flow cell. The 400bps sequencing
352 mode with a minimum read length of 200bp were selected. Gupply (v6.5.7) was used at the
353 super-accurate basecalling, demultiplexing, and adapter removal. Total long reads: 53773 with
354 89.607 % of bps > Q20.

355 To generate the completed genome, porechop (v0.2.4) was used to trim residual adapter
356 sequences from long reads. Flye (v2.9.2) was used to generate the *de novo* assembly under the
357 nano-hq model. Reads longer than the estimated N_{50} based on a genome size of 6Mbp initiated
358 the assembly. Subsequent polishing using the short read data was performed using Pilon (v1.24)
359 under default parameters. Long read contigs with an average short read coverage of 15X or less
360 were removed from the assembly. The assembled contig was confirmed to be circular via
361 circulator (v1.5.5). Annotation was performed using prokka (v 1.14.6). Finally, statistics were
362 recorded using QUAST (v5.2.0). The final genome contained 1 contig of 4750347 bp with a
363 sequencing depth of 123.92x. The N_{50} was 4750347. This genome can be accessed via the
364 accession number CP165600 or via the BioProject PRJNA1142534 via NCBI.
365 The completed genome has an estimated average nucleotide identity of 99.9694 to the W3110
366 genome deposited to NCBI (genome assembly ASM1024v1).
367
368 **RNA isolation and quality control.** Cells were grown for 2 hours in 1 mL GT media. 60 µL
369 were then added to 1 mL of fresh GT, with or without 1 mM putrescine, and grown for another
370 two hours. After growth, the cells were centrifuged, and frozen at -80ºC. The isolation and
371 analysis protocol has been previously published (15). Cell pellets were thawed, resuspended in
372 0.7 mL of buffer RLT (Qiagen RNeasy kit), and mechanically lysed using a bead beater
373 (FastPrep-24 Classic from MP Biomedical) set at the highest setting for three 45-s cycles with a
374 5-min rest period on ice between cycles. Cell lysates were used to isolate RNA using a Qiagen
375 RNeasy mini kit. RNA was quantified, DNase treated, and re-quantified on a nanodrop. RNA
376 that passed the first quality check was analyzed on RNA-IQ (Qubit). RNA with an IQ higher
377 than 7.5 was used. RNA that passed both checks were run on an agarose gel to check for RNA

378 integrity. RT-qPCR was used to ensure there was no DNA contamination. RNA libraries that
379 passed all these quality checks were submitted to the genomics core facility at the University of
380 Texas at Dallas for RNA sequencing. The core performed rRNA removal (RiboMinus
381 Transcriptome Isolation Kit or RiboCop bacterial rRNA depletion—Lexogen), library
382 preparation (Stranded Total RNA Prep—Illumina), and single-end Illumina sequencing.
383
384 **Reverse transcription quantitative PCR.** RNA was isolated as described above. One
385 microgram of RNA was reverse transcribed using LunaScript RT Super Mix (NEB E3010) and
386 another microgram was subjected to the same reaction as the reverse transcribed RNA, except
387 without reverse transcriptase (negative control) following manufacturer instructions. The cDNA
388 was then diluted to 10 ng/µL for qPCR. PCR reactions were composed of 10 ng cDNA, 8 µL of
389 nuclease free water, 10 nM primers (rpoD: Forward: TCGTGTTGAAGCAGAAGAAGCG;
390 Reverse: TCGTCATCGCCATCTTCTTCG) (fimA: Forward: ATGGTGGGACCGTTCACTTT;
391 Reverse: GGCAACAGCGGCTTTAGATG), and PowerUp SYBR Green 2X master mix for
392 qPCR (ThermoFisher A25777) in a 20 µL reaction. A Quantstudio 3 qPCR machine was used to
393 generate critical threshold (Ct) values. The Ct values were then analyzed using the $2^{-\Delta\Delta C_T}$ method
394 (37) using *rpoD* as a library control.
395
396 **RNAseq Analysis.** Transcripts were aligned to the W3110 genome and CDS (CP165600)
397 available on NCBI using CLC genomics workbench (Qiagen version 22.00) for RNA-seq
398 analysis. The gene expression counts generated as this output were used to perform differentially
399 expressed gene (DEG) analysis using EdgeR (version 3.38.4) to analyze read counts (38, 39).
400 DEGs had an adjusted P-value less than 0.05.

401

402 **Data availability:** The raw RNA seq reads were deposited in GenBank: BioProject accession
403 number PRJNA1126736. The genome was deposited in GenBank: BioProject accession number
404 PRJNA1142534. The genome accession number is CP165600.

405

406 **Acknowledgements:** This work was funded through private donations. PEZ received
407 endowment support from the Cain Foundation through the Felecia and John Cain Distinguished
408 Chair in Women's Health in honor of Philippe E. Zimmern, MD. The authors declare no potential
409 conflicts of interests.

410 The authors (JH, SH, and GV) would like to thank Prof. Kelli Palmer of the University of
411 Texas at Dallas for the use of her space, supplies, and tissue homogenizer. JH would like to
412 further thank Prof. Palmer for the use of her CLC genomics program. The authors would like to
413 thank the Genome Center at The University of Texas at Dallas for the services to support our
414 research. The authors would like to thank the Olympus Discovery Center/Imaging Core facility
415 at UT Dallas for providing equipment and support (Fig. 8), and the UT Southwestern Medical
416 Center for electron microscopy (Fig. 2).

417

418

419 **References:**

420 1. Tabor CW, Tabor H. 1984. Polyamines. Annual review of biochemistry 53:749-90.
421 2. Tabor CW, Tabor H. 1984. Polyamines. Annu Rev Biochem 53:749-90.
422 3. Chattopadhyay MK, Tabor CW, Tabor H. 2009. Polyamines are not required for aerobic growth of
423 *Escherichia coli*: preparation of a strain with deletions in all of the genes for polyamine
424 biosynthesis. J Bacteriol 191:5549-52.
425 4. Igarashi K, Kashiwagi K. 2000. Polyamines: mysterious modulators of cellular functions. Biochem
426 Biophys Res Commun 271:559-64.

427 5. Igarashi K, Kashiwagi K. 2015. Modulation of protein synthesis by polyamines. IUBMB Life
428 67:160-9.
429 6. Yoshida M, Kashiwagi K, Shigemasa A, Taniguchi S, Yamamoto K, Makinoshima H, Ishihama A,
430 Igarashi K. 2004. A unifying model for the role of polyamines in bacterial cell growth, the
431 polyamine modulon. J Biol Chem 279:46008-13.
432 7. Armbruster CE, Hodges SA, Mobley HL. 2013. Initiation of swarming motility by *Proteus mirabilis*
433 occurs in response to specific cues present in urine and requires excess L-glutamine. J Bacteriol
434 195:1305-19.
435 8. Kurihara S, Suzuki H, Tsuboi Y, Benno Y. 2009. Dependence of swarming in *Escherichia coli* K-12
436 on spermidine and the spermidine importer. FEMS Microbiol Lett 294:97-101.
437 9. Sudarshan S, Hogins J, Ambagaspitiye S, Zimmern P, Reitzer L. 2021. The nutrient and energy
438 pathway requirements for surface motility of nonpathogenic and uropathogenic *Escherichia coli*.
439 J Bacteriol. doi:10.1128/jb.00467-20doi:10.1128/jb.00467-20.
440 10. Yokota T, Gots JS. 1970. Requirement of adenosine 3', 5'-cyclic phosphate for flagella formation
441 in *Escherichia* coli and *Salmonella typhimurium*. J Bacteriol 103:513-6.
442 11. Tabor CW, Tabor H. 1985. Polyamines in microorganisms. Microbiol Rev 49:81-99.
443 12. Sugiyama Y, Nakamura A, Matsumoto M, Kanbe A, Sakanaka M, Higashi K, Igarashi K, Katayama T,
444 Suzuki H, Kurihara S. 2016. A novel putrescine exporter SapBCDF of *Escherichia coli*. J Biol Chem
445 291:26343-26351.
446 13. Igarashi K, Ito K, Kashiwagi K. 2001. Polyamine uptake systems in *Escherichia coli*. Res Microbiol
447 152:271-8.
448 14. Kurihara S, Suzuki H, Oshida M, Benno Y. 2011. A novel putrescine importer required for type 1
449 pili-driven surface motility induced by extracellular putrescine in *Escherichia coli* K-12. J Biol
450 Chem 286:10185-92.
451 15. Hogins J, Xuan Z, Zimmern PE, Reitzer L. 2023. The distinct transcriptome of virulence-associated
452 phylogenetic group B2 *Escherichia coli*. Microbiol Spectr. doi:10.1128/spectrum.02085-
453 23e0208523. doi:10.1128/spectrum.02085-23.
454 16. Schneider BL, Hernandez VJ, Reitzer L. 2013. Putrescine catabolism is a metabolic response to
455 several stresses in *Escherichia coli*. Mol Microbiol 88:537-50.
456 17. Schneider BL, Reitzer L. 2012. Pathway and enzyme redundancy in putrescine catabolism in
457 *Escherichia coli*. J Bacteriol 194:4080-8.
458 18. Fukuchi J, Kashiwagi K, Yamagishi M, Ishihama A, Igarashi K. 1995. Decrease in cell viability due
459 to the accumulation of spermidine in spermidine acetyltransferase-deficient mutant of
460 *Escherichia coli*. J Biol Chem 270:18831-5.
461 19. Sakamoto A, Sahara J, Kawai G, Yamamoto K, Ishihama A, Uemura T, Igarashi K, Kashiwagi K,
462 Terui Y. 2020. Cytotoxic mechanism of excess polyamines functions through translational
463 repression of specific proteins encoded by polyamine modulon. Int J Mol Sci 21.
464 20. Schwan WR. 2011. Regulation of *fim* genes in uropathogenic *Escherichia coli*. World J Clin Infect
465 Dis 1:17-25.
466 21. Karp PD, Ong WK, Paley S, Billington R, Caspi R, Fulcher C, Kothari A, Krummenacker M,
467 Latendresse M, Midford PE, Subhraveti P, Gama-Castro S, Muniz-Rascado L, Bonavides-Martinez
468 C, Santos-Zavaleta A, Mackie A, Collado-Vides J, Keseler IM, Paulsen I. 2018. The EcoCyc
469 Database. EcoSal Plus. 8(1):doi:10.1128/ecosalplus.ESP-0006-2018.
470 22. Keseler IM, Mackie A, Santos-Zavaleta A, Billington R, Bonavides-Martínez C, Caspi R, Fulcher C,
471 Gama-Castro S, Kothari A, Krummenacker M, Latendresse M, Muñiz-Rascado L, Ong Q, Paley S,
472 Peralta-Gil M, Subhraveti P, Velázquez-Ramírez DA, Weaver D, Collado-Vides J, Paulsen I, Karp PD.

2016. The EcoCyc database: reflecting new knowledge about *Escherichia coli* K-12. Nucleic Acids Research 45:D543-D550.
23. Tabor H, Tabor CW. 1969. Partial separation of two pools of arginine in *Escherichia coli*; preferential use of exogenous rather than endogenous arginine for the biosynthesis of 1,4-diaminobutane. J Biol Chem 244:6383-7.
24. Miyamoto S, Kashiwagi K, Ito K, Watanabe S, Igarashi K. 1993. Estimation of polyamine distribution and polyamine stimulation of protein synthesis in *Escherichia coli*. Arch Biochem Biophys 300:63-8.
25. Iwadate Y, Golubeva YA, Slauch JM. 2023. Cation homeostasis: Coordinate regulation of polyamine and magnesium levels in *Salmonella*. mBio 14:e0269822.
26. Applebaum DM, Dunlap JC, Morris DR. 1977. Comparison of the biosynthetic and biodegradative ornithine decarboxylases of *Escherichia coli*. Biochemistry 16:1580-4.
27. Wu WH, Morris DR. 1973. Biosynthetic arginine decarboxylase from *Escherichia coli*. Purification and properties. J Biol Chem 248:1687-95.
28. Flores-Mireles AL, Walker JN, Caparon M, Hultgren SJ. 2015. Urinary tract infections: epidemiology, mechanisms of infection and treatment options. Nat Rev Microbiol 13:269-84.
29. Puebla-Barragan S, Renaud J, Sumarah M, Reid G. 2020. Malodorous biogenic amines in *Escherichia coli*-caused urinary tract infections in women-a metabolomics approach. Sci Rep 10:9703.
30. Satink HP, Hessels J, Kingma AW, van den Berg GA, Muskiet FA, Halie MR. 1989. Microbial influences on urinary polyamine excretion. Clin Chim Acta 179:305-14.
31. Keay SK, Birder LA, Chai TC. 2014. Evidence for bladder urothelial pathophysiology in functional bladder disorders. Biomed Res Int 2014:865463.
32. Alteri CJ, Smith SN, Mobley HL. 2009. Fitness of *Escherichia coli* during urinary tract infection requires gluconeogenesis and the TCA cycle. PLoS Pathog 5:e1000448.
33. Baba T, Ara T, Hasegawa M, Takai Y, Okumura Y, Baba M, Datsenko KA, Tomita M, Wanner BL, Mori H. 2006. Construction of *Escherichia coli* K-12 in-frame, single-gene knockout mutants: the Keio collection. Mol Syst Biol 2:2006 0008.
34. Miller JH. 1972. Experiments in Molecular Genetics. Cold Spring Harbor Laboratory, Cold Spring Harbor, NY.
35. Datsenko KA, Wanner BL. 2000. One-step inactivation of chromosomal genes in *Escherichia coli* K-12 using PCR products. Proc Natl Acad Sci U S A 97:6640-5.
36. Hogins J, Zimmern PE, Reitzer L. 2023. Genome sequences of seven clade B2 *Escherichia coli* strains associated with recurrent urinary tract infections in postmenopausal women. Microbiol Resour Announc doi:10.1128/mra.00035-23:e0003523.
37. Livak KJ, Schmittgen TD. 2001. Analysis of relative gene expression data using real-time quantitative PCR and the 2(-Delta Delta C(T)) Method. Methods 25:402-8.
38. McCarthy DJ, Chen Y, Smyth GK. 2012. Differential expression analysis of multifactor RNA-Seq experiments with respect to biological variation. Nucleic Acids Res 40:4288-97.
39. Robinson MD, McCarthy DJ, Smyth GK. 2010. edgeR: a Bioconductor package for differential expression analysis of digital gene expression data. Bioinformatics 26:139-40.

Table 1. Differentially expressed genes that are proposed to contribute to putrescine homeostasis. A positive number means more transcripts in the Δ*speB* (lower putrescine) strain.

517

518

Gene (function)	log_2FC	FDR
Polyamine synthesis		
speA (putrescine)	0.99	0.003
speC (putrescine)	1.43	3E-4
speD (spermidine)	-0.83	0.01
speF (putrescine)	1.05	0.007
rpmH (inhibitor of SpeA and SpeC)	-2.77	2E-4
rpsT (inhibitor of SpeA and SpeC)	-1.92	8E-4
Polyamine transport		
*potABCD** (spermidine)	-2.17	3E-4
potE (putrescine)	2.07	2E-4
*potFGHI** (putrescine)	1.41	4E-4
plaP (putrescine)	1.11	0.005
*sapBCDF** (putrescine export)	-1.18	8E-4
Arginine synthesis		
argA_2 (synthesis)	1.77	0.001
argB (synthesis)	1.87	0.002
argC (synthesis)	2.86	0.005
argD (synthesis)	1.41	0.001
argF (synthesis)	1.63	0.01
argG (synthesis)	2.32	0.002
argH (synthesis)	0.97	0.001
argI (synthesis)	1.95	0.018
argR (repressor of arginine regulon)	-1.33	4E-4

Glutamate generation		
glsA (glutamine degradation)	2.16	5E-4
glnG (regulation of ammonia assimilation)	-1.59	0.022
TCA cycle/electron transport		
acnA (TCA cycle)	-1.04	8E-4
acnB (TCA cycle)	-1.96	2E-4
fumA (TCA cycle)	-1.50	6E-4
fumB (TCA cycle)	-1.49	0.003
gltA (TCA cycle)	-1.64	2E-4
icdA (TCA cycle)	-1.32	0.002
*sdhCDAB-sucABCD** (TCA cycle)	-3.88	5E-5
nuo operon* (electron transport)	-0.82	0.004
*menFDHBCE** (electron transport)	-0.8	0.005
*ubiEJB** (electron transport)	-0.93	0.004
*cyoABCD** (electron transport)	-1.41	9E-4
*hemCD** (heme)	-2.05	2E-4
Iron transport		
*exbBD** (transport of all iron chelates)	-2.33	4E-5
tonB (transport of all iron chelates)	-1.9	4E-5
*entCEBA** (enterochelin iron)	-5.2	7E-6
fecABCDE * (ferric citrate)	-4.4	3E-5
fecIR (regulators, ferric citrate)	-4.4	6E-6
*feoABC** (ferrous iron)	-3.4	7E-4
fur (regulator, iron assimilation)	-0.40	0.11
Magnesium and phosphate transport		
mgtA (magnesium)	5.90	5E-6

phoQ (regulator, magnesium)	0.79	0.009
*pstSCAB** (phosphate)	3.61	0.01
*phoBR** (regulator, phosphate assimilation)	2.80	0.02

519

520 * Values for transcripts of the first gene of operon are given. Results for other genes of the
521 operon are in Supplemental Table 1

522

523

524 Table 1. Strains

Strain Name	Genotype	Reference
BLS77	W3110 Δ*puuR*::*cat*	(17)
BLS80	W3110 Δ*puuA*::*cat*	(17)
BLS88	W3110 Δ*patA* Δ*puuA*	(17)
CP2	W3110 Δ*patA*	(17)
IM26	W3110 Δ*speB::kan fliC-lacZ*	This study
IM27	W3110 Δ*speE::kan fliC-lacZ*	This study
IM28	W3110 Δ*speF::cat fliC-lacZ*	This study
IM29	W3110 Δ*speC::kan fliC-lacZ*	This study
IM34	W3110 Δ*speC* Δ*speF::cat fliC-lacZ*	This study
IM60	W3110 Δ*cadA::kan fliC-lacZ*	This study
IM61	W3110 Δ*speA::kan*	This study
IM62	W3110 Δ*patA* Δ*puuA* Δ*speE::kan*	This study
IM63	W3110 Δ*potE::kan*	This study
IM64	W3110 Δ*potF::kan*	This study
IM65	W3110 Δ*plaP::kan*	This study
IM66	W3110 Δ*puuP::kan*	This study
J15	W3110 Δ*speB* Δ*fliC*::*kan*	This study
SA1	W3110 Δ*fliC::kan*	This study

SA2	W3110 Δ*fimA::kan*	This study
SA3	W3110 Δ*fliC* Δ*fimA*	This study
SA4	W3110 Δ*hns::kan*	This study
SA5	W3110 Δ*ihfA::kan*	This study
SA6	W3110 Δ*lrp::kan*	This study
W3110-LR	*lacI*^{q} *lacL8*	Lab strain

525 **Figure legends:**

526 Figure 1 Pathways and enzymes of polyamine synthesis.

527

528 Figure 2. Surface motility of W3110-LR. (A) Surface motility of parental and derivative strains
529 lacking the major subunits of the flagella (FliC), pili (FimA), or both. (B) Swimming motility with
530 and without 0.5% glucose. (C) TEM images of cells of W3110-LR and W3110-LR Δ*fliC* Δ*fimA*
531 taken from the movement's edge directly from surface motility plates.

532

533 Figure 3. Genetics of surface motility. (A) PDSM of mutants with defects in polyamine anabolic
534 genes. (B) Diameter of surface movement of polyamine mutants after 36 hours. Error bars
535 represent standard deviations for three independent replicates. Statistical analysis was performed
536 using the Dunnett test of significance: *, $P<0.05$; **, $P<0.01$; ***, $P<0.001$. All assays were
537 performed in triplicate and representative images are shown. In this figure the Δ*speB* mutant was
538 IM26.

539

540 Figure 4: Nutritional supplementation of Δ*speB* mutant. (A) Putrescine and spermidine
541 supplementation of wild type and Δ*speB* strains. (B) Diameter of surface movement of
542 polyamine mutants after 36 hours. Error bars represent standard deviations for three independent
543 replicates. Statistical analysis was performed using the Sadik test of significance: *, $P<0.05$; **,
544 $P<0.01$; ***, $P<0.001$. All assays were performed in triplicates and representative images are
545 shown. In this figure the Δ*speB* mutant was IM26.
546
547 Figure 5: Putrescine transport and surface motility. (A) Representative images of surface motility
548 for strains defective in putrescine transport genes. (B) Diameter of surface movement of
549 polyamine mutants after 36 hours. Error bars represent standard deviations for three independent
550 replicates. Statistical analysis was performed using the Dunnett test of significance: *, $P<0.05$;
551 **, $P<0.01$; ***, $P<0.001$. All assays were performed in triplicate and representative images are
552 shown.
553
554 Figure 6: Putrescine catabolism and surface motility. (A) Pathways and enzymes of putrescine
555 catabolism. (B) Motility diameter of putrescine catabolic mutants after 36 hours. Error bars
556 represent standard deviations for three independent replicates. Statistical analysis was performed
557 using the Dunnett test of significance: *, $P<0.05$; **, $P<0.01$; ***, $P<0.001$. All assays were
558 performed in triplicates and representative images are shown. (C) Effect of loss of *speE* on the
559 *patA puuA* catabolic double mutant.
560
561 Figure 7: Surface motility and pili expression in W3110 and Δ*speB*. (A) W3110 Δ*speB* surface
562 motility with 0.0, 0.1, 1.0, and 4.0 mM exogenous putrescine. All assays were performed in

563 triplicate. Representative images are shown. (B) Average diameter of 3 separate surface motility
564 plates. The parental strain without putrescine is shown for reference. Significance was
565 determined by comparing the diameters of the Δ*speB* mutants in the different concentrations of
566 putrescine compared to the parental W3110. One way ANOVA was used with Dunnett
567 hypothesis testing to determine p values, ***, $p < 0.001$. (C) Reverse transcriptase-quantitative
568 PCR using primers targeting the *fimA* gene from cells grown in 0.0, 0.1, 1.0, and 4.0 mM of
569 supplemented putrescine. Double deltas were generated by normalizing the parental and the
570 Δ*speB* mutant RNA libraries to *rpoD* then comparing *fimA* expression. Two-way ANOVA was
571 used to determine significance followed by Sadik hypothesis testing. ***, $p<0.001$. (D) Enzyme
572 linked immunosorbent assays using antibodies targeting pili (FimA) from cells grown with 0.0,
573 0.1, 1.0, and 4.0 mM of supplemented putrescine. Two-way ANOVA was used to determine
574 significance followed by FDR adjusting. ***, $p<0.001$. In this figure the Δ*speB* mutant was J15.
575
576 Figure 8: Transmission electron micrographs of Δ*speB* mutant cells after surface motility.
577 Representative images are shown and cells were removed from motility plates with the following
578 exogenous putrescine concentrations: (A) none, (B) 0.1 mM, (C) 1.0 mM, and (D) 4.0 mM. No
579 pili were observed with 0 and 0.1 mM putrescine. Optimal pili production was observed with 1.0
580 mM putrescine. Shorter and less pili were observed with 4.0 mM. The arrows in (D) point to
581 apparent pili fragments. The bar represents one micron. In this figure the Δ*speB* mutant was J15.
582
583 Figure 9: Visual representation of the results from transcriptomic sequencing of W3110 and the
584 Δ*speB* mutant's gene expression in media with and without 1.0 mM putrescine. (A)
585 Multidimensional scaling plot of the parental and Δ*speB* mutant transcriptomes. When grown

586 with 1.0 mM putrescine (red), the Δ*speB* mutant transcriptome (triangles) are nearly identical to
587 the parental transcriptomes when grown without and with putrescine (blue and red circles,
588 respectively). When grown without putrescine, the Δ*speB* mutant transcriptome (blue triangles)
589 is greatly skewed from transcriptomes of the parental strain and the Δ*speB* mutant grown with
590 putrescine. (B) Heatmap of the top 100 most variable genes further demonstrates the
591 distinctiveness of the Δ*speB* mutant grown without putrescine and the similarities of the Δ*speB*
592 mutant transcriptome when grown with 1.0 mM putrescine supplementation and the parental
593 grown with or without putrescine. In this figure the Δ*speB* mutant was J15.
594
595 Figure 10: Transcriptomic sequencing of genes for the *fim* region and regulators that control *fim*
596 gene expression. (A) Expression of the *fim* genes in the parental W3110 and the speB mutant
597 with and without putrescine supplementation. Values were calculated by dividing the individual
598 replicates' counts per million (CPM) value for each gene by the mean CPM of that gene in
599 W3110 grown without putrescine and multiplying by 100 to yield the percent expression. Arrows
600 below the genes signify the known operons: *fimB* and *fimE* belong to single gene operons, while
601 *fimAICDFGH* belong to one operon. One way ANOVA was used to determine significance using
602 Dunnett hypothesis testing. **, $p < 0.01$; ***, $p < 0.001$. (B) Expression of some regulators
603 known to affect *fim* gene expression. Values were calculated as described in (A). ***, $p < 0.001$.
604 (C) Surface motility of W3110 and three regulator mutants (Δ*hns*, Δ*ihfA*, and Δ*lrp*). A gene found
605 to be significantly different by this transcriptomic analysis (*hns*) was confirmed to be important in
606 surface motility.
607 In this figure the Δ*speB* mutant was J15.
608

609 Figure 11: The deduced diversion of metabolism in a *speB* mutant away from energy metabolism
610 toward putrescine synthesis compared to the parental strain. The effects of low putrescine are
611 shown. Genes and processes (transport and transcriptional regulators) in red have fewer
612 transcripts, while those in black or blue have more. The dashed lines represent proposed
613 reduction in metabolic flux because of fewer transcripts from genes coding for the enzymes
614 involved. Operons are shown except for the larger operons or regulons. For example, pur is
615 meant to represent the unlinked genes that code for enzymes of purine synthesis. Table 1 or
616 Supplemental Table 1 should be consulted for specific genes and the quantitative change in
617 transcripts.
618
619 Supplemental Figure 1: Growth and swimming of polyamine anabolic mutants. (A) Growth
620 curves of wild type and putrescine deficient mutants in a shaking aerobic culture. (B)
621 Representative images of swimming.
622
623 Supplemental Table 1. Supplemental Table 1: Differential gene expression analysis of W3110
624 and Δ*speB*. J15 refers to the Δ*speB* mutant. In the tab labeled "W3110_0_vs_J15_1_ Putrescine"
625 W3110 was grown without putrescine, J15 was grown with 1.0 mM putrescine; positive fold
626 change values refer to increases in J15 gene expression.
627
628 Supplementary Figure 2: Expression graphs comparing the logCPM of the transcriptomes of the
629 average of the three replicates of the W3110 with and without 1 mM putrescine and the speB
630 mutant with and without 1 mM putrescine. A regression line was calculated and the correlation

631 between each set of transcriptomes noted on the graph. Higher R2 values indicate greater

632 similarity between the transcriptomes.

Figure 1

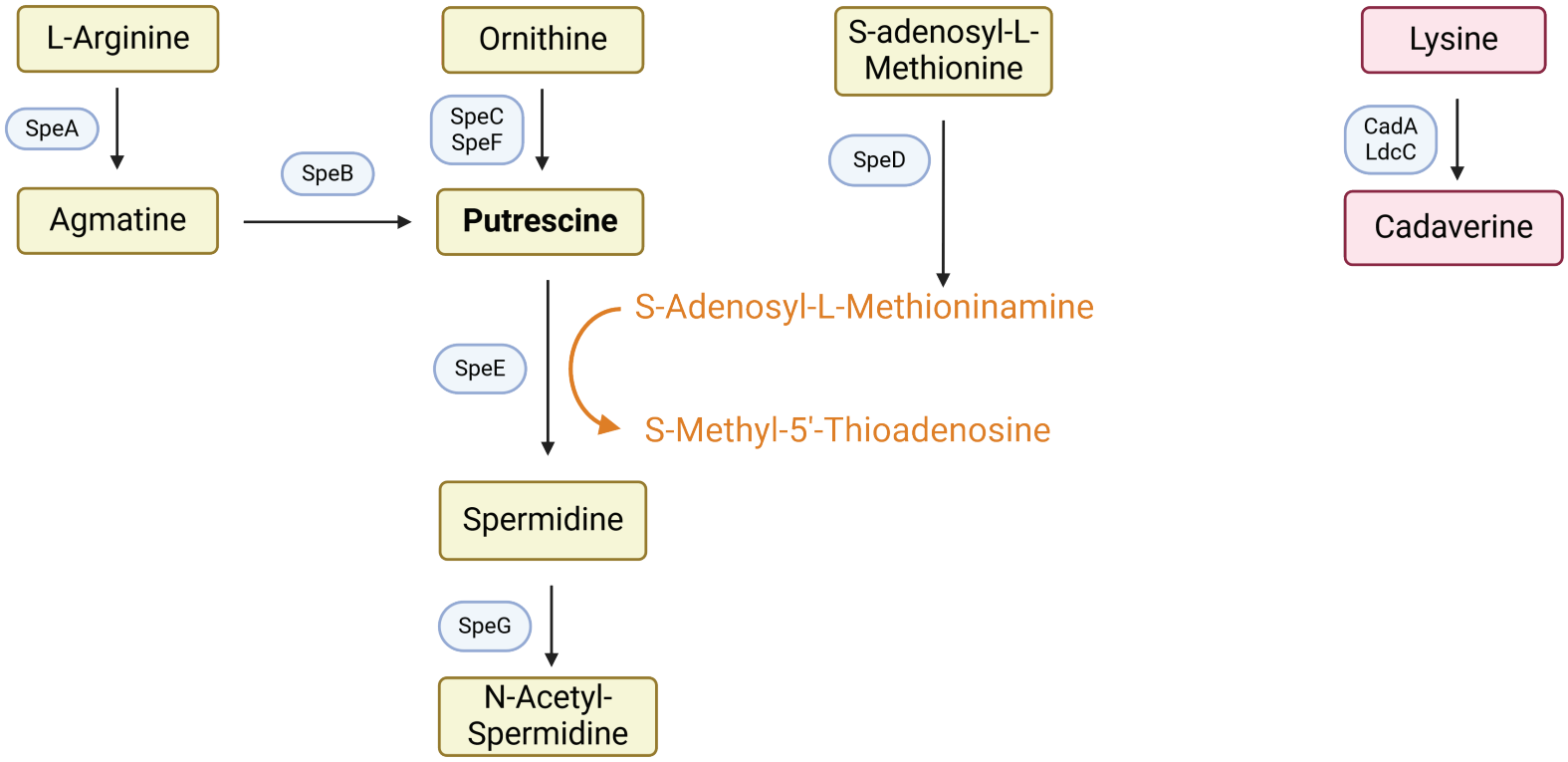

Figure 1 Pathways and enzymes of polyamine synthesis.

Figure 2

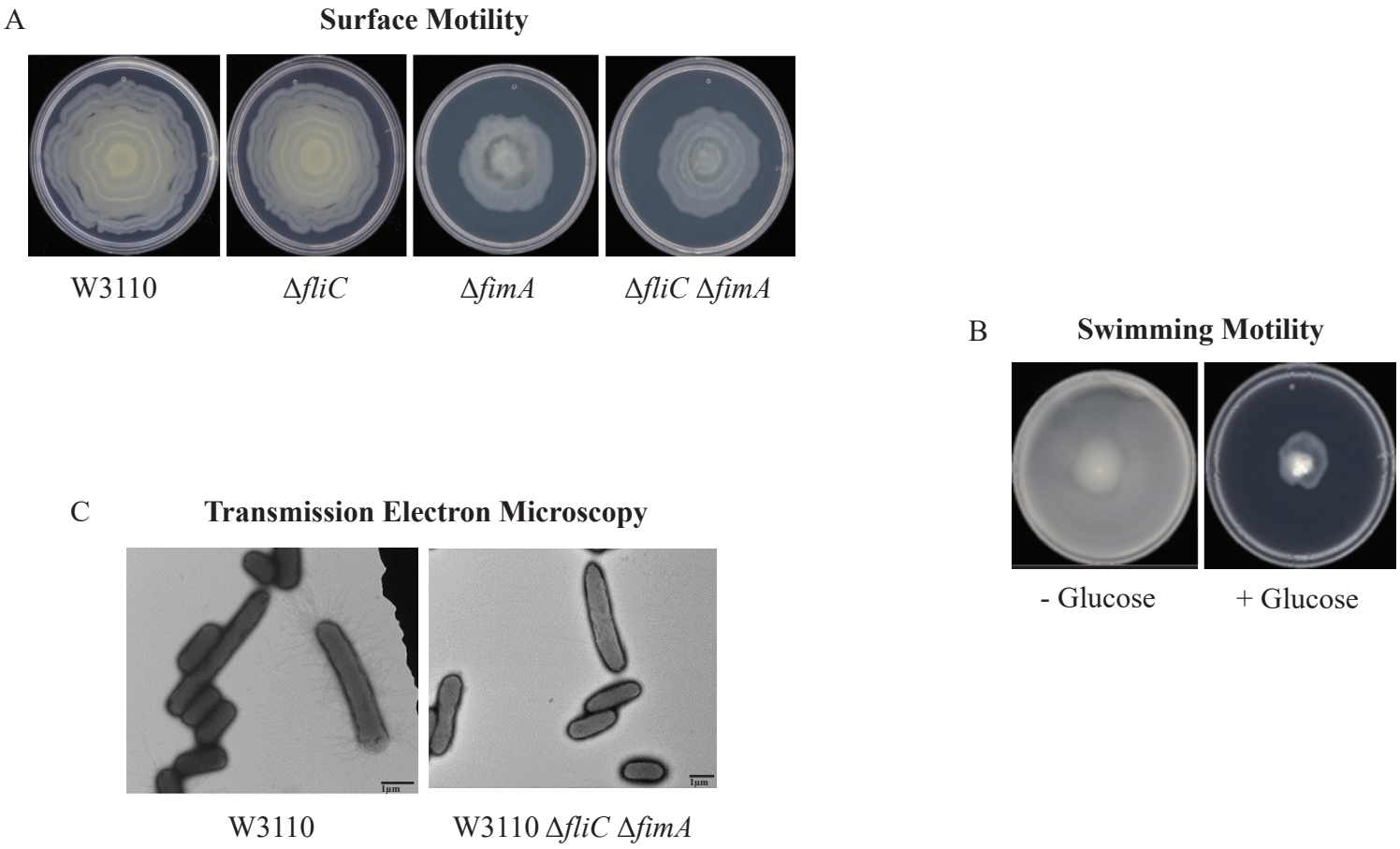

Figure 2. Surface motility of W3110-LR. (A) Surface motility of parental and derivative strains lacking the major subunits of the flagella (FliC), pili (FimA), or both. (B) Swimming motility with and without 0.5% glucose. (C) TEM images of cells of W3110-LR and W3110-LR Δ*fliC* Δ*fimA* taken from the movement's edge directly from surface motility plates.

Figure 3

A

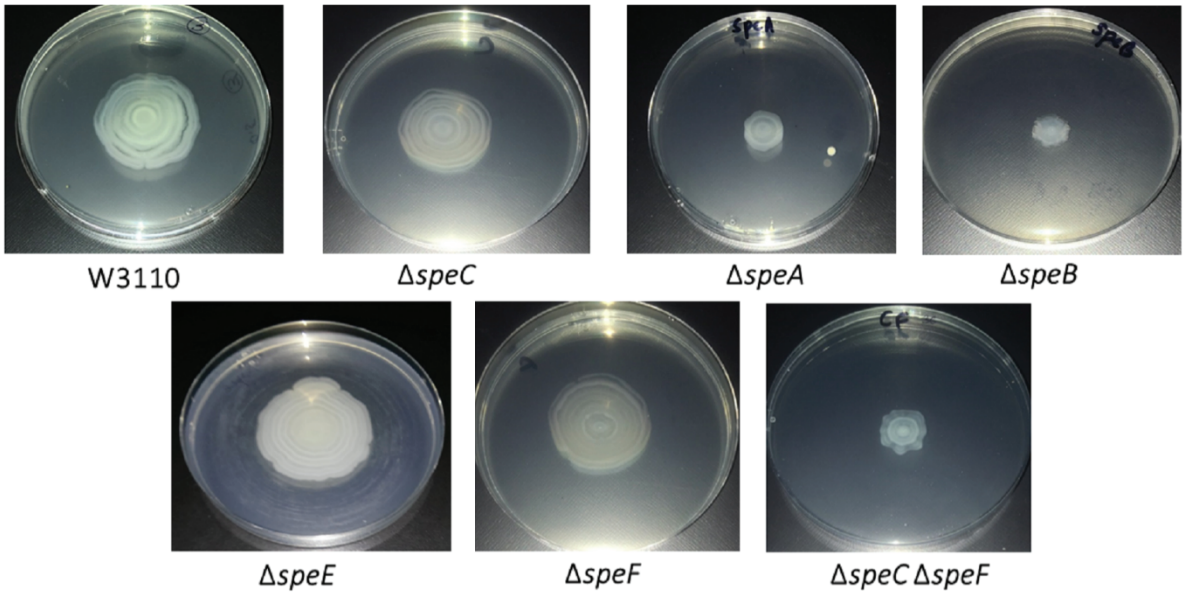
W3110
ΔspeC
ΔspeA
ΔspeB
ΔspeE
ΔspeF
ΔspeC ΔspeF

B

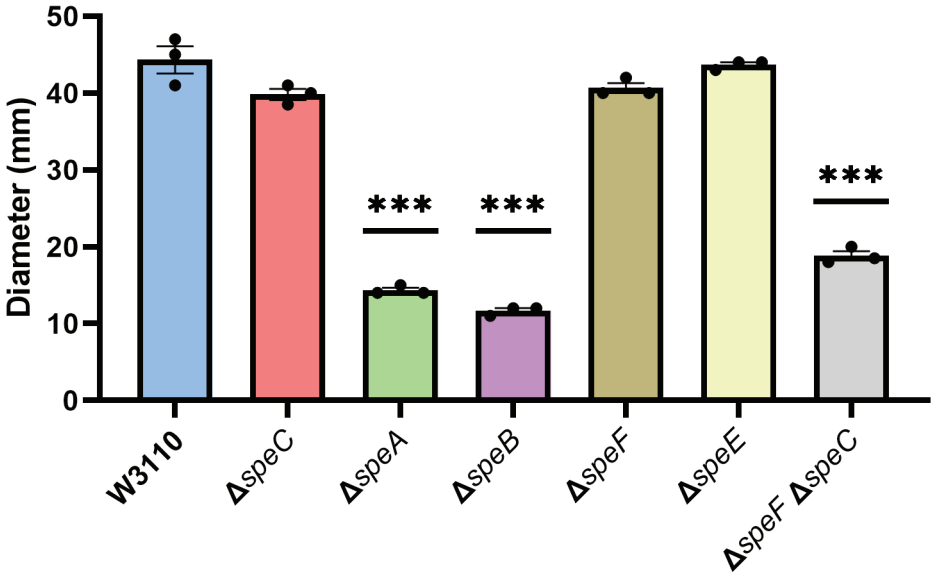
Diameter (mm)
50
40
30
20
10
0
***
***
***
W3110
ΔspeC
ΔspeA
ΔspeB
ΔspeF
ΔspeE
ΔspeF ΔspeC

Figure 3 Legend

Figure 3. Genetics of surface motility. (A) PDSM of mutants with defects in polyamine anabolic genes. (B) Diameter of swarm colonies of polyamine mutants after 36 hours. Error bars represent standard deviations for three independent replicates. Statistical analysis was performed using the Dunnett test of significance: *, $P<0.05$; **, $P<0.01$; ***, $P<0.001$. All assays were performed in triplicates and representative images are shown. In this figure "Δ*speB*" refers to IM26.

Figure 4

A

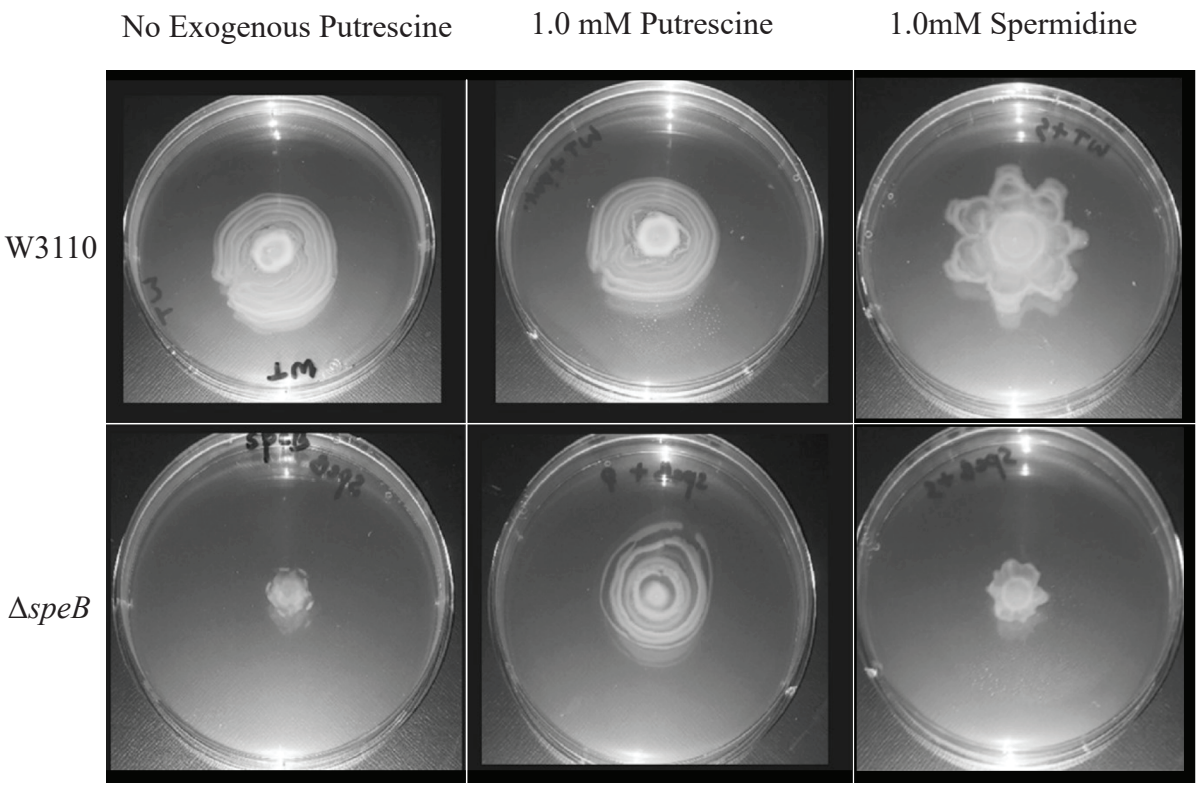
No Exogenous Putrescine
1.0 mM Putrescine
1.0mM Spermidine
W3110
ΔspeB

B

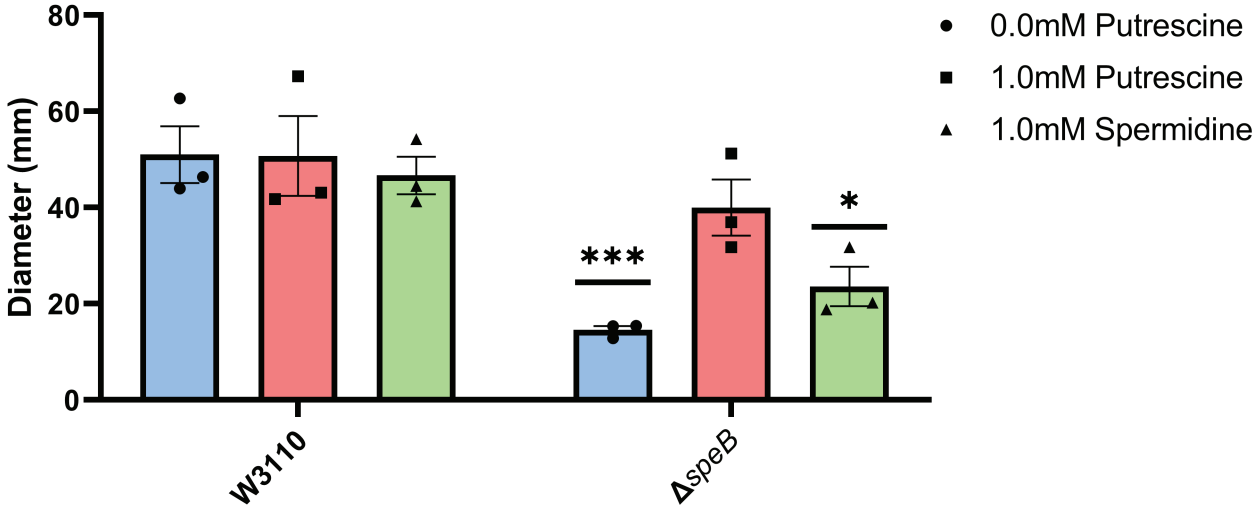
80
60
40
20
0
Diameter (mm)
***
*
W3110
ΔspeB
0.0mM Putrescine
1.0mM Putrescine
1.0mM Spermidine

Figure 4 Legend

Figure 4: Nutritional supplementation of Δ*speB* mutant. (A) Putrescine and spermidine supplementation of wild type and Δ*speB* strains. (B) Diameter of swarm colonies of polyamine mutants after 36 hours. Error bars represent standard deviations for three independent replicates. Statistical analysis was performed using the Sadik test of significance: *, $P<0.05$; **, $P<0.01$; ***, $P<0.001$. All assays were performed in triplicates and representative images are shown. In this figure "Δ*speB*" refers to IM26.

Figure 5

A

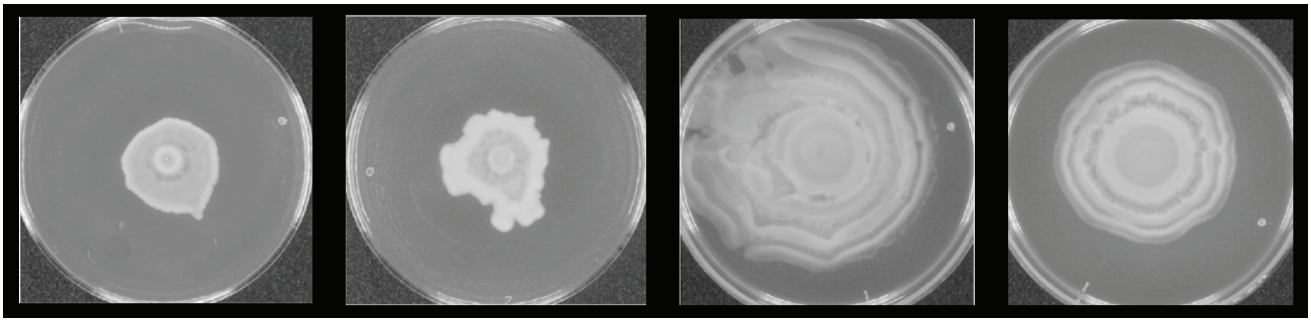

ΔplaP *ΔpotF* *ΔpotE* *ΔpuuP*

B

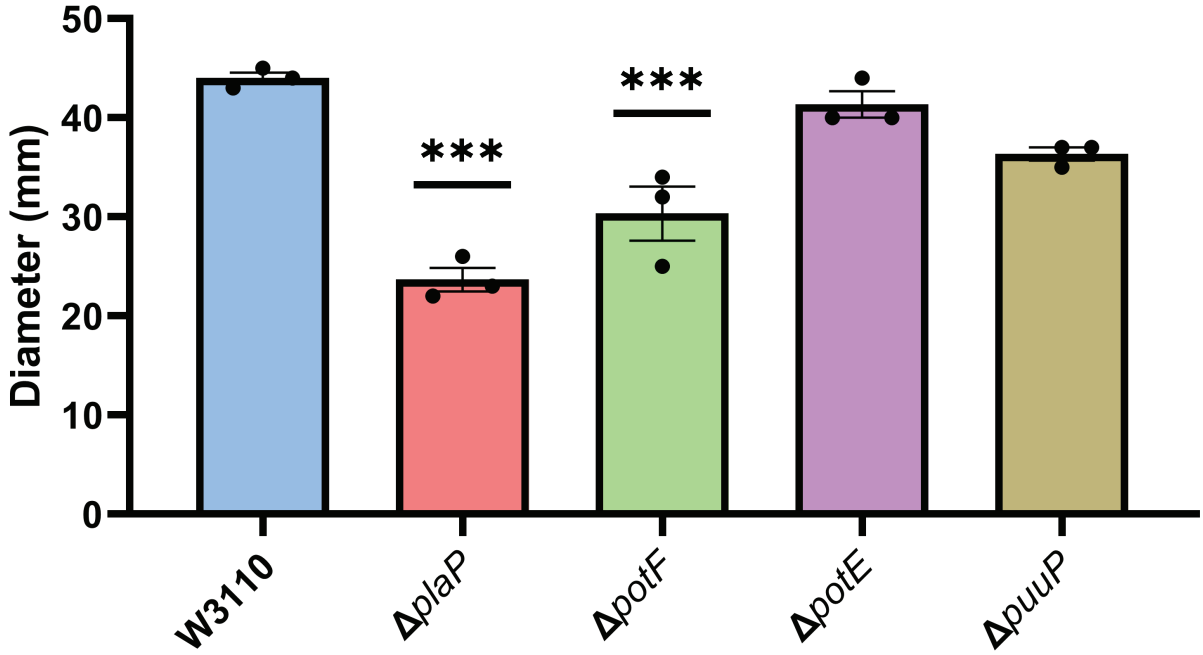

Figure 5: Putrescine transport and surface motility. (A) Representative images of swarming for strains defective in putrescine transport genes. (B) Diameter of swarm colonies of polyamine mutants after 36 hours. Error bars represent standard deviations for three independent replicates. Statistical analysis was performed using the Dunnett test of significance: *, $P<0.05$; **, $P<0.01$; ***, $P<0.001$. All assays were performed in triplicates and representative images are shown.

Figure 6

A

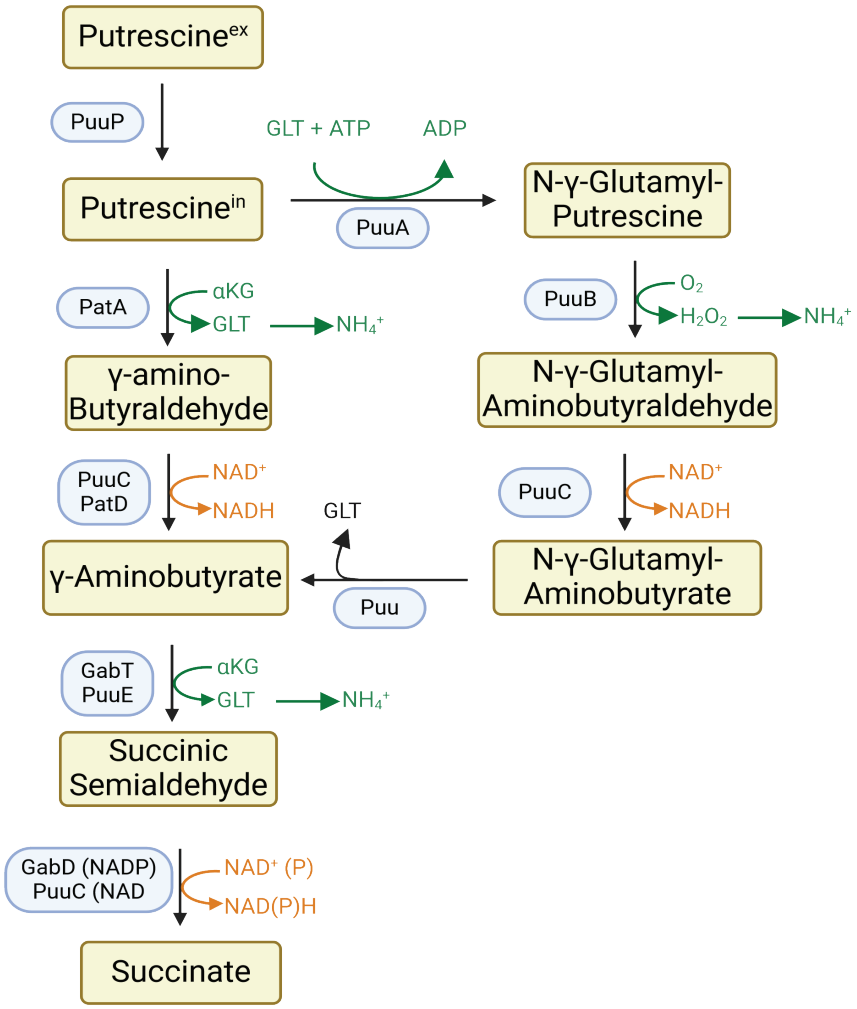

B

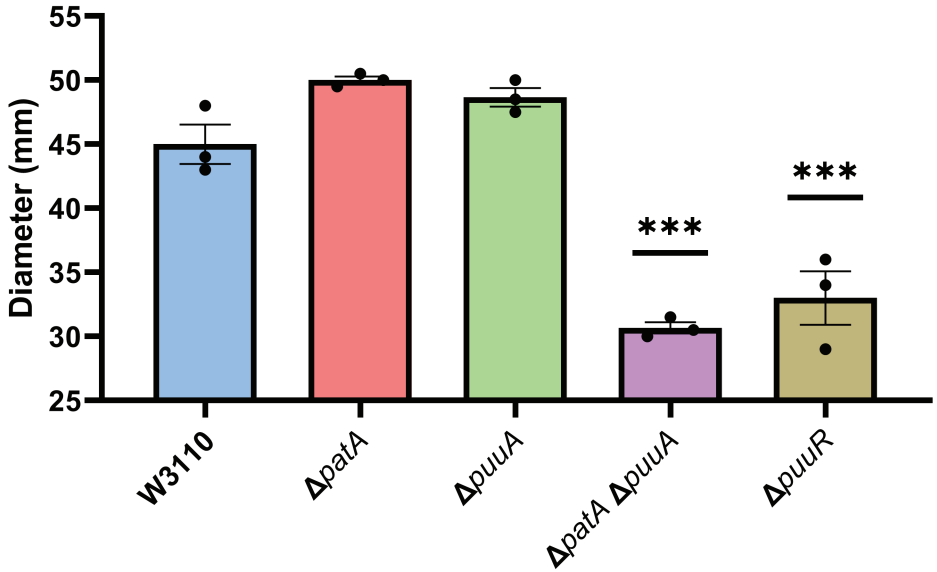

C

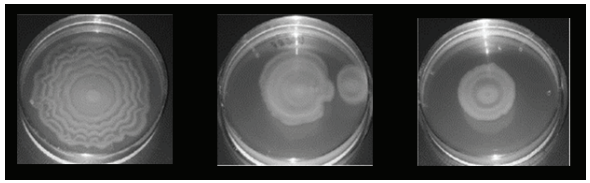

W3110 *ΔpatA ΔpuuA* *ΔpatAΔpuuA ΔspeE*

Figure 6 Legend

Figure 6: Putrescine catabolism and surface motility. (A) Pathways and enzymes of putrescine catabolism. (B) Motility diameter of putrescine catabolic mutants after 36 hours. Error bars represent standard deviations for three independent replicates. Statistical analysis was performed using the Dunnett test of significance: *, $P<0.05$; **, $P<0.01$; ***, $P<0.001$. All assays were performed in triplicates and representative images are shown. (C) Effect of loss of *speE* on the *patA puuA* catabolic double mutant.

Figure 7

A

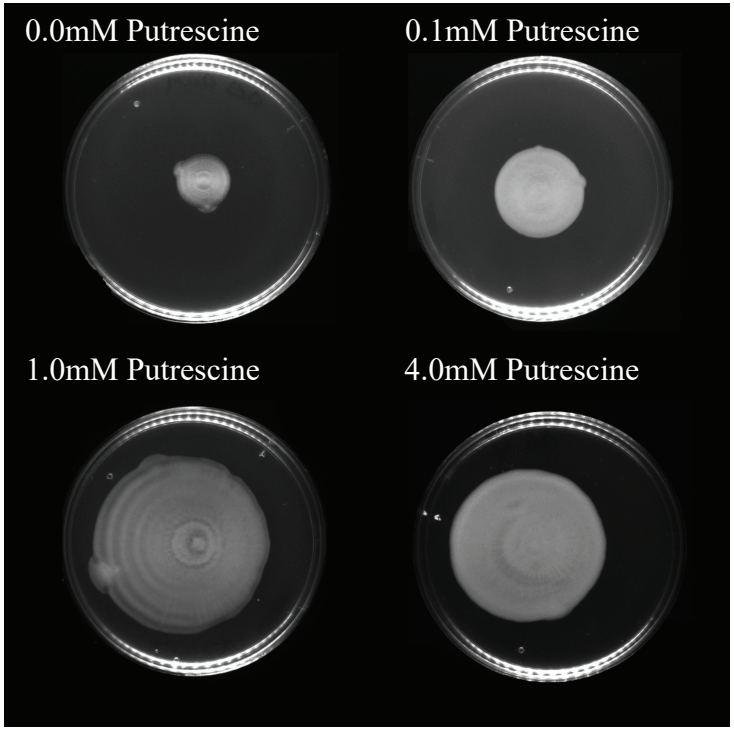

B

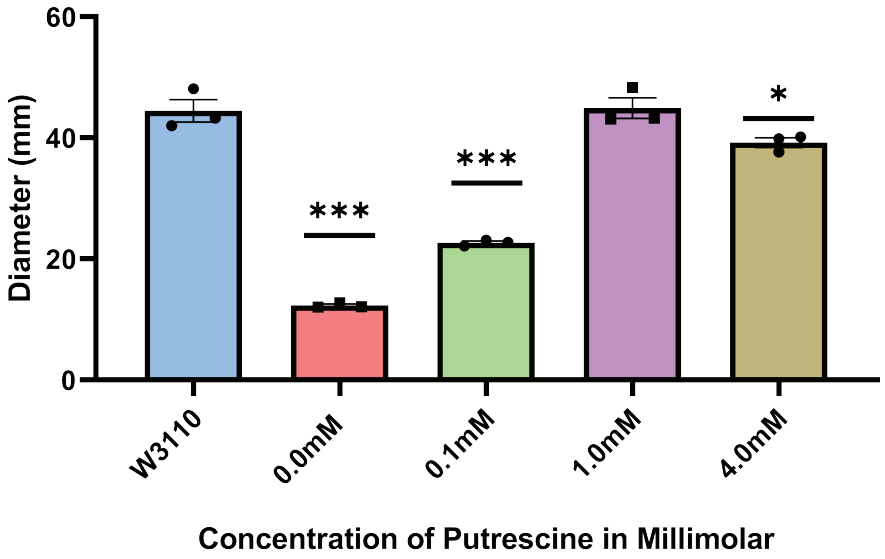

C

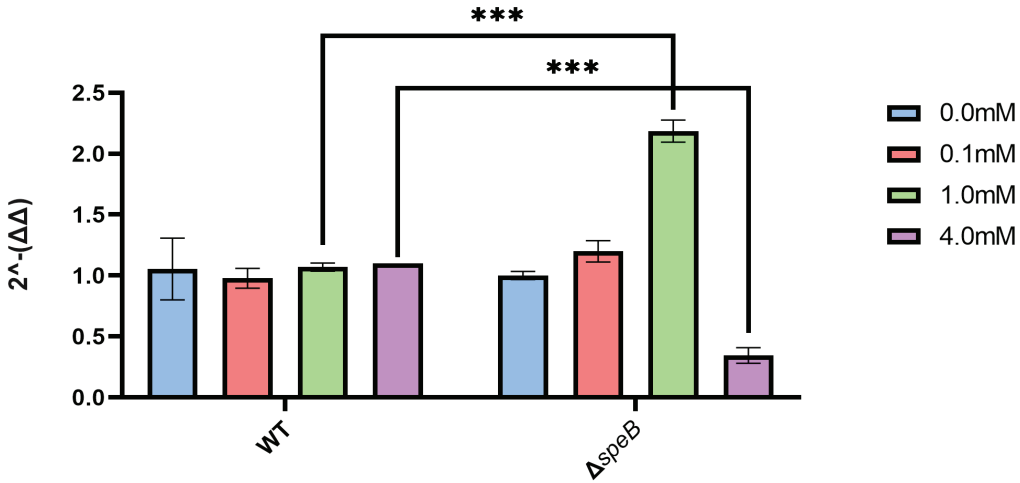

D

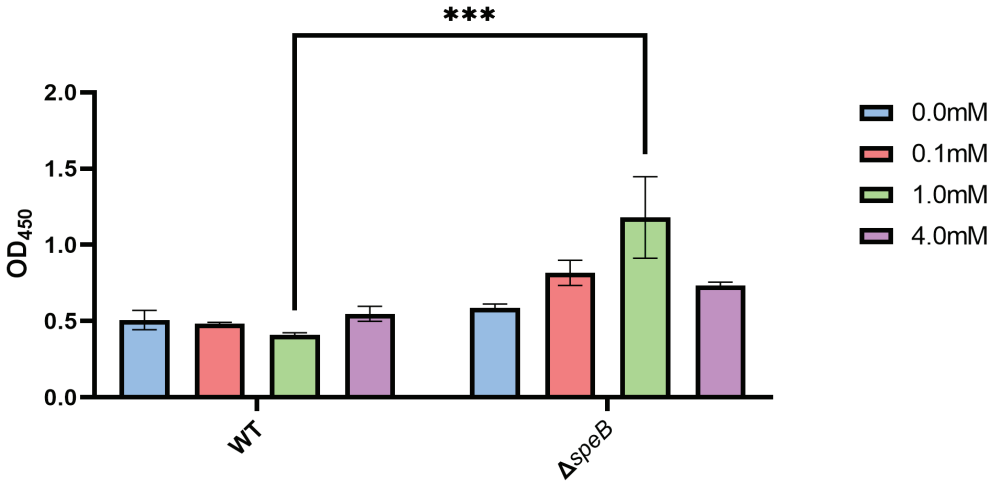

Figure 7 Legend

Figure 7: Surface motility and pili expression in W3110 and Δ*speB*. (A) W3110 Δ*speB* surface motility with 0.0, 0.1, 1.0-, and 4.0-mM exogenous putrescine. All assays were performed in triplicate. Representative images are shown. (B) Average diameter of 3 separate surface motility plates. The parental strain without putrescine is shown for reference. Significance was determined by comparing the diameters of the Δ*speB* mutants in the different concentrations of putrescine compared to the parental W3110. One way ANOVA was used with Dunnett hypothesis testing to determine p values. ***, $p < 0.001$. (C) Reverse transcriptase-quantitative PCR using primers targeting the *fimA* gene from cells grown in 0.0, 0.1, 1.0, and 4.0 mM of supplemented putrescine. Double deltas were generated by normalizing the parental and the Δ*speB* mutant RNA libraries to *rpoD* then comparing *fimA* expression. Two-way ANOVA was used to determine significance followed by Sidak hypothesis testing. ***, $p<0.001$. (D) Enzyme linked immunosorbent assays using antibodies targeting pili (FimA) from cells grown with 0.0, 0.1, 1.0, and 4.0 mM of supplemented putrescine. Two-way ANOVA was used to determine significance followed by FDR adjusting. ***, $p<0.001$. In this figure "Δ*speB*" refers to J15.

Figure 8

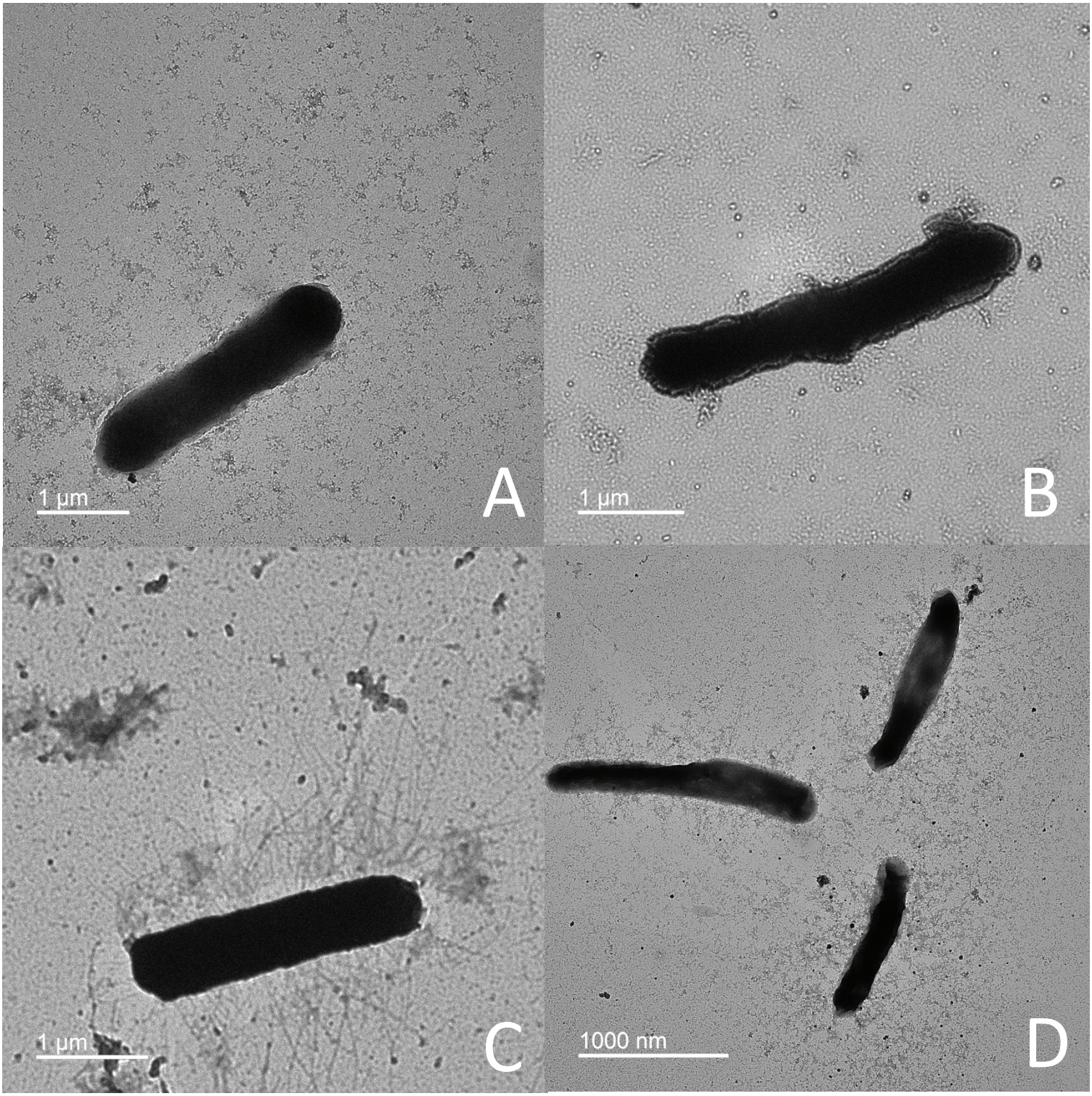

Figure 8 Legend

Figure 8: Transmission electron micrographs of Δ*speB* mutant cells after surface motility. Representative images are shown and cells were removed from motility plates with the following exogenous putrescine concentrations: (A) none, (B) 0.1 mM, (C) 1.0 mM, and (D) 4.0 mM. No pili were observed with 0, and 0.1 mM putrescine. Optimal pili production was observed with 1.0 mM putrescine. Shorter and less pili were observed with 4.0 mM. The arrows in (D) point to apparent pili fragments. The bar represents one micron. The bar represents one micron. In this figure "Δ*speB*" refers to J15.

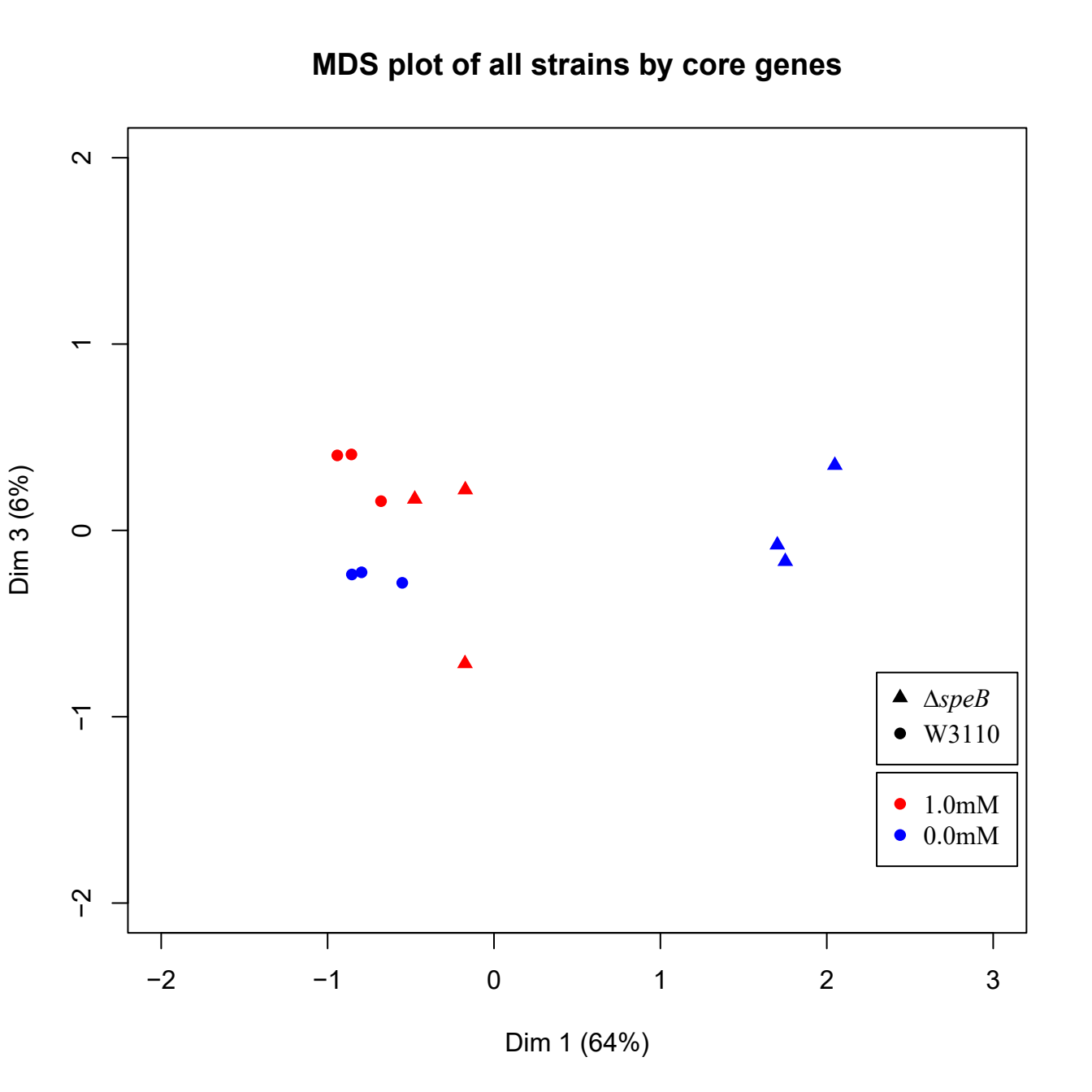
MDS plot of all strains by core genes
Dim 3 (6%)
Dim 1 (64%)
2
1
0
−1
−2
−2
−1
0
1
2
3
ΔspeB
W3110
1.0mM
0.0mM

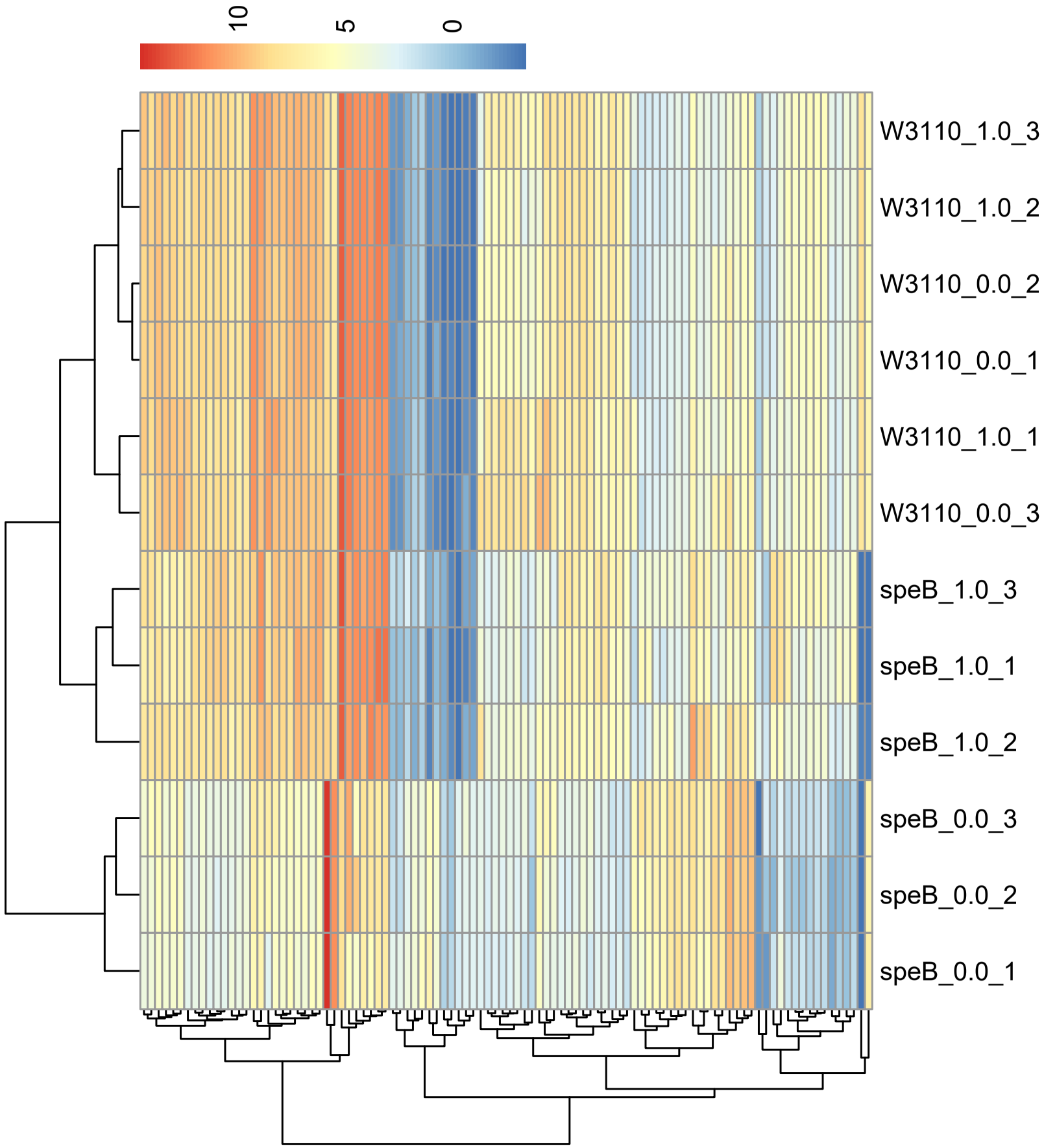
10
5
0
W3110_1.0_3
W3110_1.0_2
W3110_0.0_2
W3110_0.0_1
W3110_1.0_1
W3110_0.0_3
speB_1.0_3
speB_1.0_1
speB_1.0_2
speB_0.0_3
speB_0.0_2
speB_0.0_1

Figure 9 Legend

Figure 9: Visual representation of the results from transcriptomic sequencing of W3110 and the Δ*speB* mutant's gene expression in media with and without 1.0 mM putrescine. (A) Multidimensional scaling plot of the parental and Δ*speB* mutant transcriptomes. When grown with 1.0 mM putrescine (red), the Δ*speB* mutant transcriptome (triangles) are nearly identical to the parental transcriptomes when grown without and with putrescine (blue and red circles, respectively). When grown without putrescine, the Δ*speB* mutant transcriptome (blue triagles) is greatly skewed from transcriptomes of the parental strain and the Δ*speB* mutant grown with putrescine. (B) Heatmap of the top 100 most variable genes further demonstrates the distinctiveness of the Δ*speB* mutant grown without putrescine and the similarities of the Δ*speB* mutant transcriptome when grown with 1.0 mM putrescine supplementation and the parental grown with or without putrescine. In this figure "Δ*speB*" refers to J15.

Figure 10

A

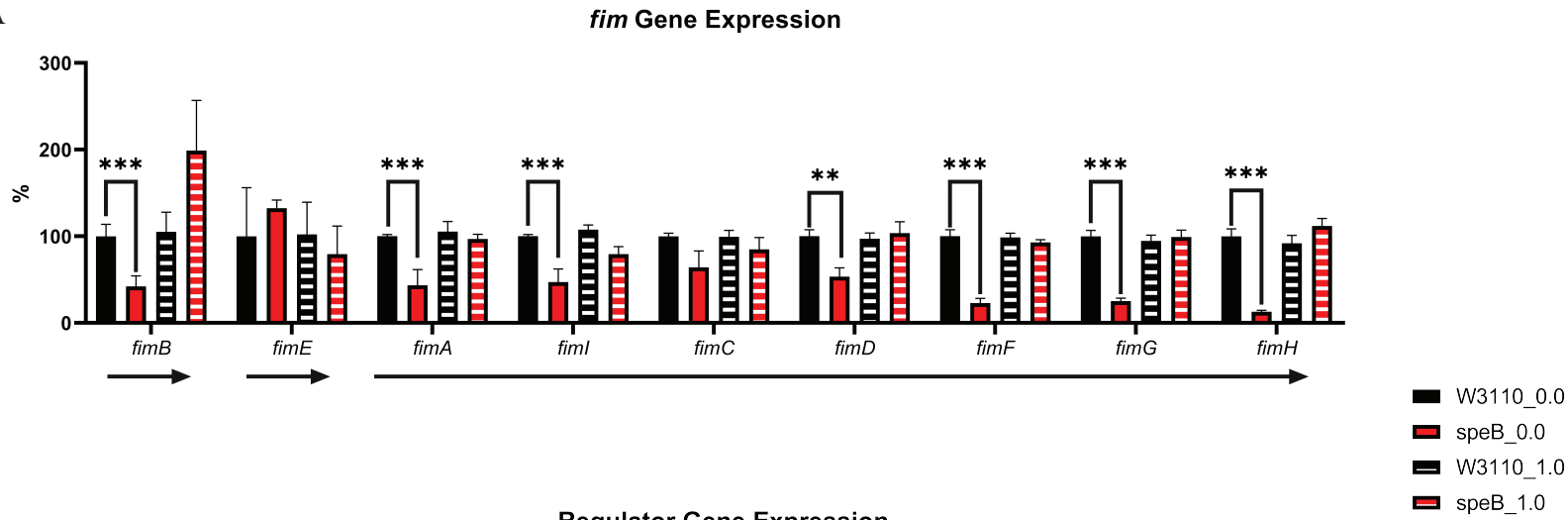

B

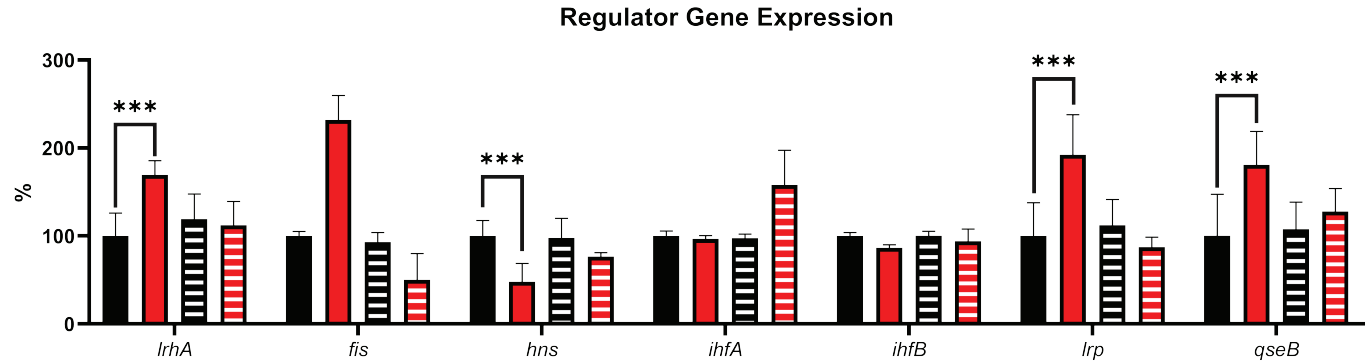

C

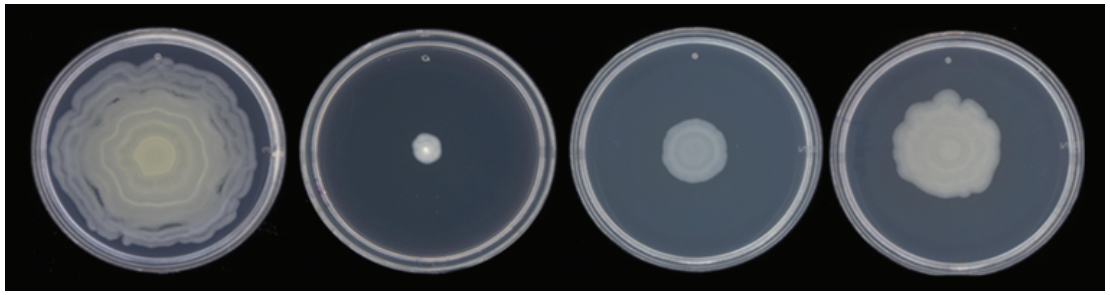

W3110 Δ*hns* Δ*ihfA* Δ*lrp*

Figure 10 Legend

Figure 10: Transcriptomic sequencing of genes for the *fim* region and regulators that control *fim* gene expression. (A) Expression of the *fim* genes in the parental W3110 and the speB mutant with and without putrescine supplementation. Values were calculated by dividing the individual replicates' counts per million (CPM) value for each gene by the mean CPM of that gene in W3110 grown without putrescine and multiplying by 100 to yield the percent expression. Arrows below the genes signify the known operons: *fimB* and *fimE* belong to single gene operons, while *fimAICDFGH* belong to one operon. One way ANOVA was used to determine significance using Dunnet hypothesis testing. **, $p < 0.01$; ***, $p < 0.001$. (B) Expression of some regulators known to affect *fim* gene expression. Values were calculated as described in (A). Two way ANOVA was used to determine significance using Sadik hypothesis testing. ***, $p < 0.001$. (C) Surface motility of W3110 and three regulator mutants (Δ*hns*, Δ*ihfA*, and Δ*lrp*). A gene found to be significant by the transcriptomic analysis (*hns*) was confirmed to be important in surface motility.

In this figure "Δ*speB*" refers to J15.

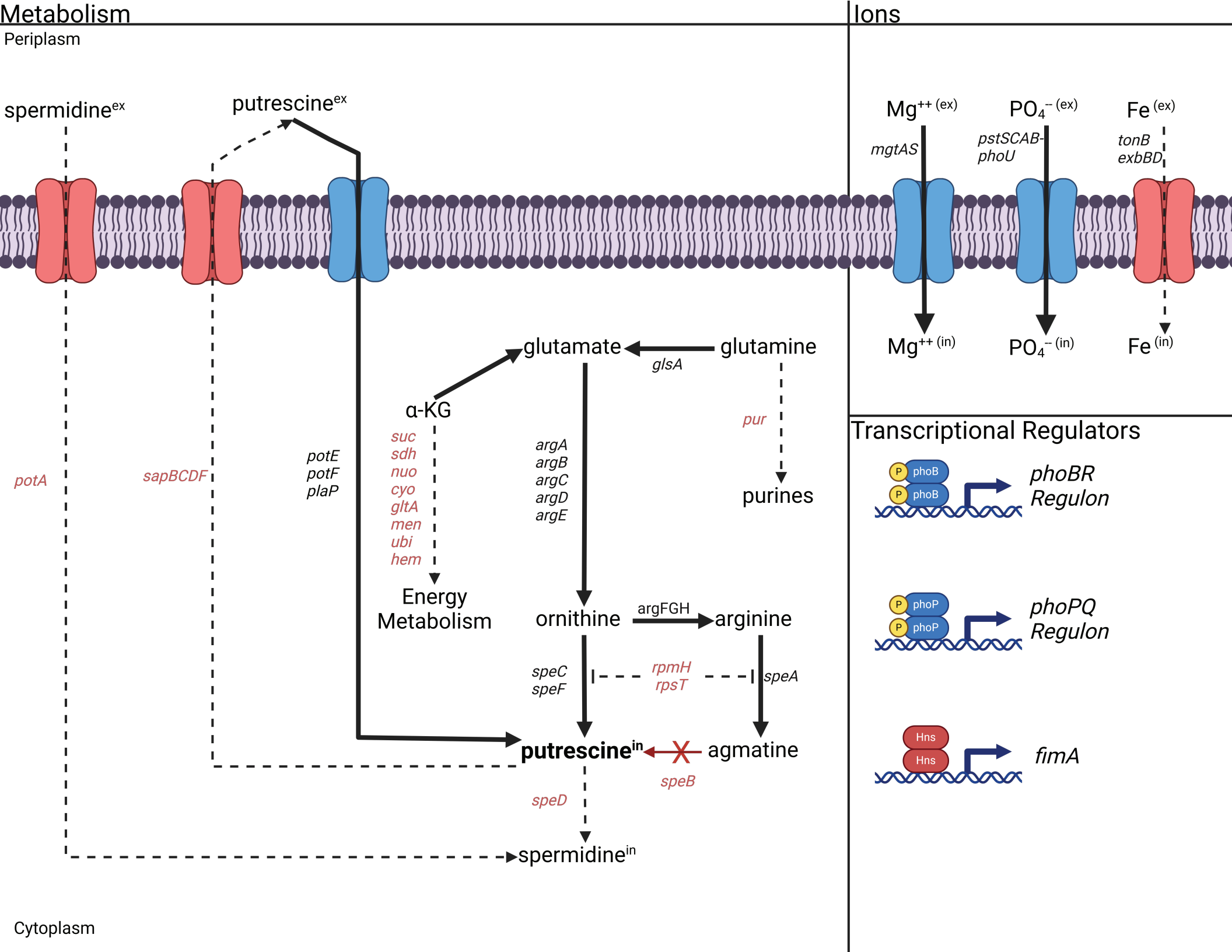
Metabolism
Periplasm
spermidine^ex
putrescine^ex
glutamate
glutamine
glsA
α-KG
pur
purines
suc
sdh
nuo
cyo
gltA
men
ubi
hem
Energy Metabolism
argA
argB
argC
argD
argE
potE
potF
plaP
potA
sapBCDF
ornithine
argFGH
arginine
speC
speF
rpmH
rpsT
speA
putrescine^in
agmatine
speB
speD
spermidine^in
Cytoplasm
Ions
Mg++ (ex)
PO4-- (ex)
Fe (ex)
mgtAS
pstSCAB-phoU
tonB exbBD
Mg++ (in)
PO4-- (in)
Fe (in)
Transcriptional Regulators
P phoB
P phoB
phoBR Regulon
P phoP
P phoP
phoPQ Regulon
Hns
Hns
fimA

Figure 11 Legned

Figure 11: The deduced diversion of metabolism in a *speB* mutant away from energy metabolism toward putrescine synthesis compared to the parental strain. The effects of low putrescine are shown. Genes and processes (transport and transcriptional regulators) in red have fewer transcripts, while those in black or blue have more. The dashed lines represent proposed reduction in metabolic flux because of fewer transcripts from genes coding for the enzymes involved. Operons are shown except for the larger operons or regulons. For example, pur is meant to represent the unlinked genes that code for enzymes of purine synthesis. Table 1 or Supplemental Table 1 should be consulted for specific genes and the quantitative change in transcripts.